T.R.
BOLU ABANT İZZET BAYSAL UNIVERSITY
INSTITUTE OF GRADUATE STUDIES
Department of Physics

FABRICATION AND APPLICATION OF BIOSENSOR FOR EARLY DIAGNOSIS OF LYMPHOMA CANCER AND CANCER METASTASIS

DOCTOR OF PHILOSOPHY

UMUTCAN GÜRER

ACADEMIC SUPERVISOR
Prof. Dr. Ercan YILMAZ

BOLU, TEMMUZ - 2023

APPROVAL OF THE THESIS

Fabrication and Application of Biosensor For Early Diagnosis of Lymphoma Cancer and Cancer Metastasis submitted by **Umutcan GÜRER** and defended before the Examining Committe Members listed below in partial fulfillment of the requirements for the degree of **Doctor of Philosophy** in **Department of Physics, Institute of Graduate Studies of Bolu Abant Izzet Baysal University in 25.07.2023** by

Examining Committee Members	**Signature**
Supervisor Prof. Dr. Ercan YILMAZ BAIBU	.....
Member Prof. Dr. Ekrem GÜREL BAIBU	.....
Member Prof. Dr. Aliekber AKTAĞ BAIBU	.....
Member Prof. Dr. Ayşegül KAHRAMAN Bursa Uludağ University	.....
Member Prof. Dr. Kadir GÖKŞEN Düzce University	.....

Prof. Dr. İbrahim KÜRTÜL

Director of Institute of Graduate Studies

ETHICAL DECLARATION

In this thesis dissertation that was properly prepared according to the Thesis Writing Rules of Bolu Abant İzzet Baysal University of the Institute of Graduates Studies, I hereby declare that;

- All data, information, and documents presented in the thesis were obtained in accordance with the academic and ethical rules,
- All data, documents, assessments, and results were presented in accordance with the scientific ethical and moral rules,
- All works that were benefitted in the thesis were appropriately cited,
- No alteration was made in the data used,
- Study presented in this thesis is original,

Otherwise, I declare that I accept the loss of all my rights in case any contradiction that may arise against me.

The similarity rate obtained by using the Turnitin program, a plagiarism detection software, is within the limits approved by the University Senate.

_____

Umutcan GÜRER

ABSTRACT

FABRICATION AND APPLICATION OF BIOSENSOR FOR EARLY DIAGNOSIS OF LYMPHOMA CANCER AND CANCER METASTASIS
PHD THESIS
UMUTCAN GÜRER
BOLU ABANT IZZET BAYSAL UNIVERSITY
INSTITUTE OF GRADUATE STUDIES
DEPARTMENT OF PHYSICS
(SUPERVISOR: PROF. DR. ERCAN YILMAZ)

BOLU, JULY 2023
xiv + 66 Pages

Lymphoma cancer ranked as the fifth cancer type is seen all around the world and death caused by lymphoma shows increment day after day. To prevention of death caused by lymphoma cancer, in the conducted study we fabricated rGO-FET biosensor device for early detection of lymphoma cancer. To do so, we synthesized the reduced graphene oxide from bulk graphite as sensing area. The fabrication of FET base structure was done by using microelectronic technology and rGO was transferred onto FET structure for use as sensing area. The characterization of rGO was completed by investigation XRD, Raman, FTIR and TEM analysis. These analysis results showed that synthesized rGO is suitable for detection. The first trials of rGO-FET biosensor were completed with various pH solutions. The pH trials revealed that the capability of rGO-FET biosensor device. For the early detection of lymphoma, the miRNA sequences were used for functionalization. The probe sequence was immobilized onto rGO sensing area for the miRNA studies. miRNA-155 sequence was dropped onto probe sequence and electrical measurements has been completed by analyzing I-V curves. The I-V curves revealed that the probe sequence immobilized on rGO matched with various concentration contained miRNA-155 sequence samples and shift was observed towards to left side with increasing concentration. The specificity study revealed that the probe sequence only matched with miRNA-155 sequence. The selectivity studies showed that rGO-FET biosensor can distinguish various concentrations. The results showed that rGO-FET can define miRNA-155 concentrations between 100 pM and 10 μM. The Limit of detection (LOD) was determined as 100 pM. Overall results suggested that the rGO-FET biosensor device successfully fabricated and can be used for early detection of lymphoma cancer and cancer metastasis.

KEYWORDS: *Biosensor, Cancer, Lymphoma, Early Detection, rGO-FET*

ÖZET

LENFOMA KANSERİ VE KANSER METASTAZININ ERKEN TEŞHİSİ İÇİN BİYOSENSÖR ÜRETİMİ VE UYGULAMASI
DOKTORA TEZİ
UMUTCAN GÜRER
BOLU ABANT İZZET BAYSAL ÜNİVERSİTESİ
LİSANSÜSTÜ EĞİTİM ENSTİTÜSÜ
FİZİK ANABİLİM DALI
(TEZ DANIŞMANI: PROF. DR. ERCAN YILMAZ)

BOLU, TEMMUZ - 2023
xiv + 66 sayfa

Dünyada beşinci sırada yer alan lenfoma kanseri tüm dünyada görülmekte ve lenfoma kaynaklı ölümler her geçen gün artış göstermektedir. Lenfoma kanserinin neden olduğu ölümleri önlemek için, yapılan çalışmada lenfoma kanserinin erken teşhisi için rGO-FET biyosensör cihazı üretilmiştir. Bunun için, algılama alanı olarak yığın grafitten indirgenmiş grafen oksit sentezlenmiştir. FET taban yapısının imalatı mikroelektronik teknolojisi kullanılarak yapıldı ve rGO algılama alanı olarak kullanılmak üzere FET yapısına aktarılarak kullanıldı. rGO'nun karakterizasyonu XRD, Raman, FTIR ve TEM analizleri incelenerek tamamlanmıştır. Bu analiz sonuçları, sentezlenen rGO'nun algılama için uygun olduğunu göstermiştir. rGO-FET biyosensörünün ilk denemeleri çeşitli pH çözeltileri ile tamamlanmıştır. pH denemeleri, rGO-FET biyosensör cihazının kullanılabilirliğini ortaya çıkarmıştır. Lenfomanın erken tespiti için miRNA dizileri işlevselleştirme için kullanılmıştır. miRNA çalışmaları için, prob dizisi rGO algılama alanı üzerine immobilize edildi. miRNA-155 dizisi prob dizisi üzerine damlatılmış ve I-V eğrileri analiz edilerek elektriksel ölçümler tamamlanmıştır. I-V eğrileri, rGO üzerinde immobilize edilen prob dizisinin çeşitli konsantrasyonlarda miRNA-155 dizisi içeren örneklerle eşleştiğini ve artan konsantrasyonla birlikte sol tarafa doğru kayma gözlendiğini ortaya koymuştur. Özgüllük çalışması, prob dizisinin sadece miRNA-155 dizisi ile eşleştiğini ortaya koymuştur. Seçicilik çalışmaları, rGO-FET biyosensörünün çeşitli konsantrasyonları ayırt edebildiğini göstermiştir. Sonuçlar, rGO-FET'in 100 pM ile 10 μM arasındaki miRNA-155 konsantrasyonlarını tanımlayabildiğini göstermiştir. LOD 100 pM olarak belirlenmiştir. Genel sonuçlar, rGO-FET biyosensör cihazının başarıyla üretildiğini ve lenfoma kanseri ve kanser metastazının erken tespiti için kullanılabileceğini göstermiştir.

ANAHTAR KELİMELER: *Biyosensör, Kanser, Lenfoma, Erken Teşhis, rGO-FET*

TABLE OF CONTENTS

LIST OF FIGURES

Page

LIST OF TABLES

Page

LIST OF PICTURES

Page

LIST OF ABBREVIATIONS AND SYMBOLS

QCM **:** Quartz Crystal Microbalance

SPR : Surface Plasmon Resonance

FET : Field Effect Transistor

CVD : Chemical Vapor Deposition

GO : Graphene Oxide

rGO : Reduced Graphene Oxide

POC : Point-of-Care

MOSFET : Metal-Oxide-Semiconductor Field Effect Transistor

GFET : Graphene Field Effect Transistor

rGO-FET : Reduced Graphene Oxide Field Effect Transistor

ISFET : Ion Sensitive Field-Effect Transistor

$\mathbf{I_{ds}}$: Drain-Source Current

$\mathbf{V_{ds}}$: Drain-Source Voltage

$\mathbf{V_{gs}}$: Gate-Source Voltage

$\mathbf{V_{Dirac}}$: Dirac Point Voltage

CNP : Charge Neutrality Point

DP : Dirac Point

$\mathbf{C_q}$: Quantum Capacitance

$\mathbf{C_{dl}}$: Double Layer Capacitance

$\boldsymbol{\varepsilon_r}$: Relative permittivity of electrolyte

$\boldsymbol{\varepsilon_o}$: Vacuum permittivity

$\boldsymbol{\lambda_D}$: Debye Length

WHO : World Healt Organization

NHL : Non-Hodgkin Lymphoma

DLBCL : Diffuse Large B-cell Lymphoma

CTC : Circulating Tumor Cells

DNA : Deoxyribonucleic Acid

RNA : Ribonucleic Acid

cf-DNA/RNA : Cell-free DNA/RNA

miRNA : Micro RNA

cf-miRNAs : Cell-free Micro RNA

LAA : L-Ascorbic Acid

XRD : X-Ray Diffraction Spectroscopy

FWHM : Full Width Half Maximum

FTIR : Fourier Transform Infrared Spectroscopy

TEM : Transmission Electron Microscopy

FET **:** Field Effect Transistor

LOD : Limit of Detection

PBS : Phosphate Buffered Saline

PBASE : 1-Pyrene butyric acid N-hydroxysuccinimide ester

PDMS : Polydimethlysiloxane

ACKNOWLEDGEMENTS

The author wishes to express his deepest gratitude to his supervisor Prof. Dr. Ercan Yılmaz for their guidance, advice, criticism, encouragements, and insight throughout the research and the opportunity to study in micro and nanoelectronics.

The author would also like to thank Prof. Dr. Aliekber Aktağ and Prof. Dr. Ekrem Gürel for their suggestions and comments throughout thesis study.

The author would also like to deeply thank Assoc. Prof. Dr. Erhan Budak and Assoc. Prof. Dr. Ercan Selçuk Ünlü and Prof. Dr. Ayşegül Kahraman for their guidance, advice and their help during experiments.

The author would like to express my sincere and endless thanks to my family who has been with me at every moment of my life, supported me in all my decisions and whose love I have always felt. And also, I would like to thank Dr. Ozan Yılmaz for his help during my academic journey, guidance and he has been always with me during entire my academic life.

This research was supported by the Higher Education Council of the Republic of Turkey within the scope of YÖK 100/2000 Doctoral Scholarship program.

1. INTRODUCTION

1.1 Biosensors

In simple terms, biosensors can be defined as device with functionalization of biological/chemical materials onto transducer materials and observing changes as electrically, optically, etc. (Thévenot et al., 2001). Biosensors have been widely used since Clark first presented them in 1962 (Clark & Lyons, 1962) for a variety of purposes, including cancer diagnosis (Balaji & Zhang, 2017; Shobha & Muniraj, 2014), toxin detection (X. Chen et al., 2018), food analysis (Ivnitski et al., 2000; Yoon & Kim, 2012), bacteria detection (Ivnitski et al., 1999) etc. In Clark's work, the biosensors were used for purpose of detecting oxygen level during surgical operations (Turner, 2013). Another illustration are the blood glucose meter and pregnancy test as Point of Care (POC) device, which are currently among the most used biosensors (Viswanathan et al., 2015). A transducer, a signal processing device, and a bio-recognition element make up the three main components of a biosensor in its most basic form (Karunakaran et al., 2015; Thévenot et al., 2001). The mechanism for converting physical quantities into signals, like as charges, mass, or photons, is initiated by the biomolecules. Transducers then convert the physical changes into a discernible electrical signal (i.e., current or voltage). The signals are ultimately processed and amplified (Bhalla et al., 2016a).

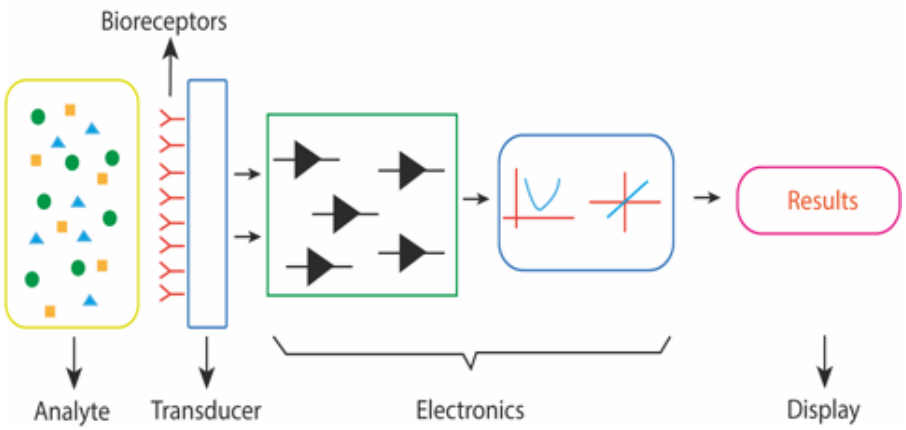

Figure 1.1. The general structure of biosensors.

The general structure of biosensors is given in Figure 1.1. The brief explanation of structures; i) the medium that contains the molecule for detection is known as an analyte, ii) a molecule that specifically recognizes the analyte is known as a bioreceptor, iii) in biosensors, the transducer's job is to convert the output of

bio-recognition into a signal that can be measured, iv) the electronics component effectively processes the transduced signal and outputs it to the display, v) The display unit primarily consists of a user interpretation system, similar to the LCD of a computer, or a printer that prints curves or figures that the customer can comprehend. Along with this structure, the usage of biosensor as POC device, they have to possess some specifications as well. The important specifications for every biosensor are given below;

1. **Selectivity:** Selectivity is perhaps the most important feature of a biosensor. Selectivity is the ability of a bioreceptor to detect a specific analyte in a sample containing other admixtures and contaminants. To construct a biosensor, selectivity is the main consideration when choosing bioreceptors (Béraud et al., 2021; Lowe et al., 2017).

2. **Sensivity:** The limit of detection (LOD) or sensitivity of a biosensor is the lowest concentration of analyte that it can detect. A biosensor is necessary in a number of medical and environmental monitoring applications to confirm the existence of traces of analytes in a sample at analyte concentrations as low as ng/ml or even fg/ml (Béraud et al., 2021; S. Li et al., 2019).
3. **Reproducibility:** The biosensor's reproducibility refers to its capacity to provide the same results under identical testing conditions. The transducer and electronics in a biosensor's are precise and accurate, which define repeatability. When a sample is tested more than once, accuracy refers to the sensor's capability to offer a mean value that is near to the real value while precision refers to the sensor's ability to produce identical findings every time (Béraud et al., 2021; Tian et al., 2020).
4. **Stability:** The stability of the biosensing system describes how sensitive it is to environmental changes both inside and outside of it. The biosensor output signals that are being monitored may wander as a result of these disruptions. This might impair the precision and accuracy of the biosensor and lead to an error in the concentration measurement. Stability is the most crucial factor when a biosensor requires prolonged incubation periods or continuous monitoring. The stability of a biosensor could be impacted by the reactivity of electronics and transducers, which may be temperature-sensitive. Because of this, accurate

electronics tuning is required to provide a constant sensor response. (Béraud et al., 2021; Hideshima et al., 2022).

1.1.1 Biosensor Types

The general categorization of biosensors is carried out by bio-recognitions material and transducer (Figure 1.2) (Mehrotra, 2016; Sawant, 2017). Some of the biosensor types as briefly;

- *Magnetic biosensors* that exploit the magnetoresistance effect to detect magnetic micro- and nanoparticles in microfluidic channels show significant potential in terms of sensitivity and size.
- The surface acoustic wave device and the quartz crystal microbalance are two different forms of *piezoelectric biosensors*. The example of this kind of biosensor is mostly used Quartz Crystal Microbalance (QCM) systems (Lim et al., 2020). They are based on the detection of variations in a piezoelectric crystal's resonance frequency driven on by changes in the mass of the crystal.

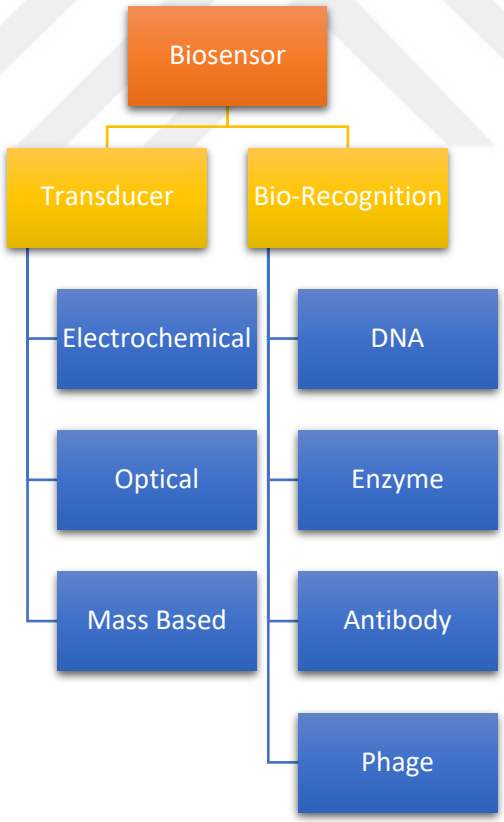

Figure 1.2. The examples of biosensor types.

- A light source, multiple optical components, and a modified sensing head and photodetector are all included in *optical biosensors***.** These components work

together to produce a light beam with specified properties that is directed toward the modulating agent. One of the most often utilized optical biosensors in literature is Surface Plasmon Resonance (SPR) (Chiu, 2022).

- Electrochemical biosensor: The detecting method used by this type of biosensor is based on converting a biological event that took place on a transducer into an electrical signal. FET (Field Effect Transistor)-based biosensors are one of the most widely used electrochemical biosensors because of their benefits, which include simple operation, quick response times, real-time monitoring without the use of labels, access to a wider variety of controlled surface chemistry approaches for anchoring bioreceptors, multiplexing abilities, and potent signal processing (Shabaninejad et al., 2019; Thévenot et al., 2001; Y. Wang et al., 2008). Numerous possibilities, including graphene and its derivatives, carbon nanotubes, carbon quantum dots, MoS_2, and others, can be found in the channel that runs between the source and drain contacts (Figure 1.3) (Aspermair et al., 2020; Sarkar et al., 2014; Shoorideh & Chui, 2012; Tran & Mulchandani, 2016). Current trend among FET biosensors is towards to graphene-based FET (GFET). The detailed information about GFET is given in next section.

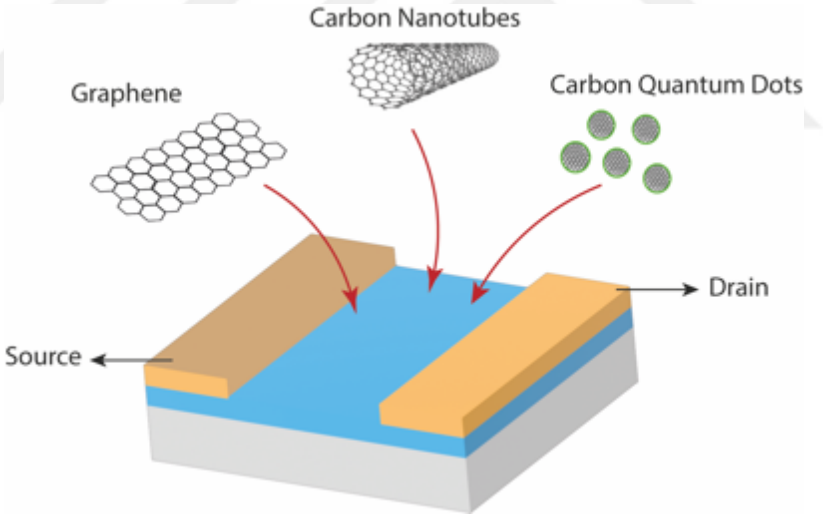

Figure 1.3. FET biosensor device structure.

1.2 Graphene Field Effect Transistors (GFET)

The graphene field effect transistor (GFET) is one of the electrochemical FET biosensors that is gaining interest from researchers worldwide due to the characteristics outlined in the preceding section. The structure of GFET is very similar to classical MOSFET structure. Three terminals—the drain, source, and gate—make up the traditional MOSFET structure (Rosenfeld et al., 1996). On the

other hand, the GFET structure differs from classical MOSFET in some manners. The main components of GFET (Figure 1.4) are i) graphene channel lies between source and drain, ii) drain and source contact and iii) the gate contact to modulation of voltage for response. The differences of the basis are the graphene channel instead of semiconducting materials and gate contacts. As sensing layer, graphene channel is used for immobilization of biological materials such as enzymes, antibodies, nucleic acids (Yazdanparast et al., 2020; Yin, 2018). By attaching receptor molecules to the particular target of interest, the GFET channel's surface is functionalized. Target molecules that bind to the receptor on the graphene surface affect the electric field throughout the FET channel area, which alters the electrical conductivity of the channel and the responsiveness of the device as a whole (Gao et al., 2020; Kwong Hong Tsang et al., 2019a; von Lüders et al., 2023). Microelectrodes are employed in the sensor for an external circuit to measure the conductance of the channel material according to its size. The main component of the sensor and factor that dictates sensor performance is the channel material, which is typically a semiconducting substance (Johnson & Mutharasan, 2014).

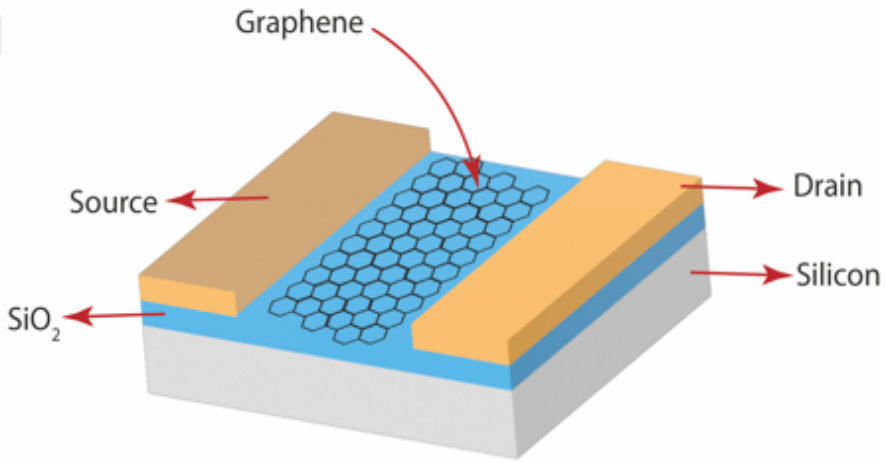

Figure 1.4. The illustration of Graphene Field Effect Transistor (GFET).

There are two formations of GFET which are back gate and top gate (Figure 1.5). In back gate, the back side of silicon is covered with also Au/Ti structure. In back gate formation, a highly conductive silicon substrate that is positioned below an insulating SiO_2 dielectric layer is commonly gated to a variety of voltages to allow the electric field to regulate the carrier density and, consequently, the conductivity of the channel (Szunerits et al., 2023). In the top gate formation is also

called as solution gate GFET that the modulation voltage of the gate is given by many different electrodes for example Ag/AgCl reference electrode. However, in some works the platinum wires and gold electrodes can be used (Fu et al., 2017; H. E. Kim et al., 2019; Kireev et al., 2017; Zhang et al., 2020). In the solution gate GFET, the voltage applied via electrode is much lower compared to back gate GFETs. The application of lower voltage prevents the water splitting and harming biomolecules in analyte (Szunerits & Boukherroub, 2018).

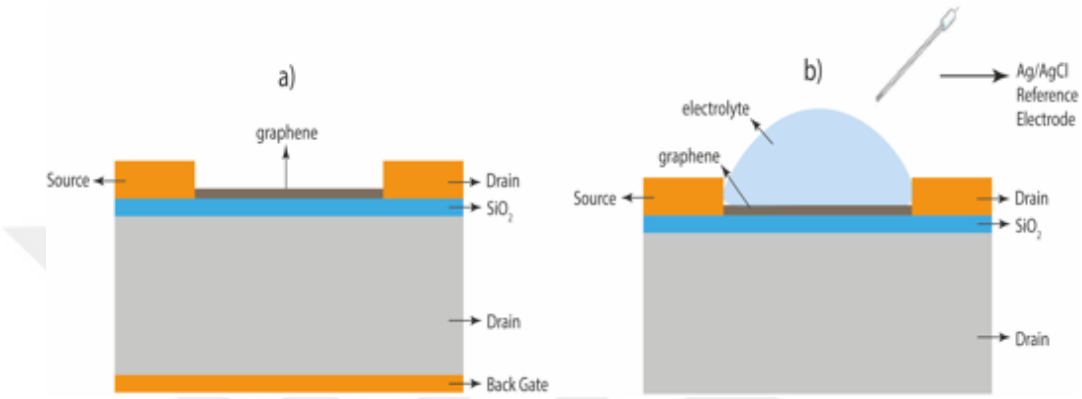

Figure 1.5. The GFET with a) back gate formation and b) top gate formation.

The Figure 1.6 shows the typical transfer characteristics of GFET. When a gate voltage (V_G) is applied, an electric field is created on the graphene channel that modifies the conductivity of the material and, as a result, the drain-source current. The redistribution of electronic charge that occurs when a target molecule attaches to the receptor on the graphene surface causes a change in the electric field throughout the FET channel area, which alters the electronic conductivity in the channel and the responsiveness of the device as a whole.

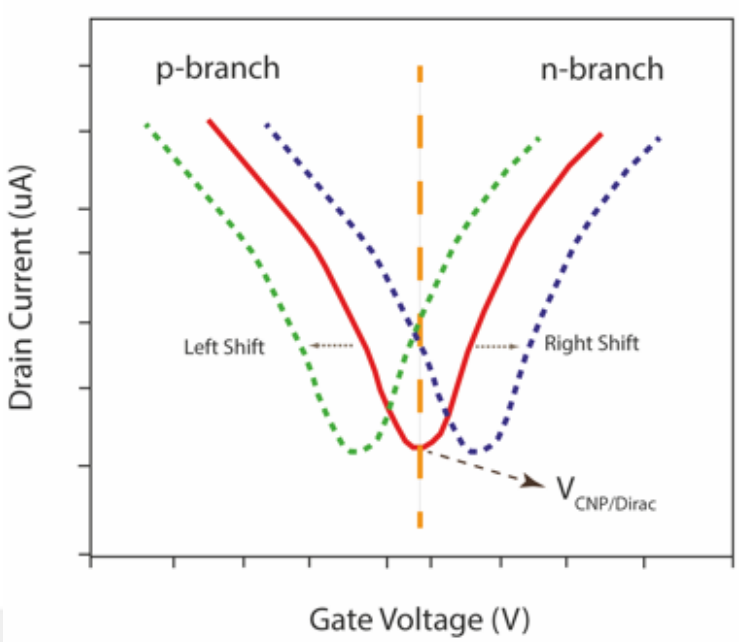

Figure 1.6. The illustration of transfer characteristics of GFET.

In addition, the sensitive detection of bioreceptor-analyte binding events in a GFET is connected to graphene doping effects via direct charge transfer between the generated bioreceptor-analyte duplex and the graphene channel, as well as electrostatic gating effects. Gating effects are attributed to the buildup of charges on the graphene surface as a result of the binding of bioreceptors and analytes, which causes a local external voltage drop across the channel. In general, positively charged analytes cause V_{Dirac} to shift to greater negative gate voltages. The density of holes in graphene will rise as a result of the negatively charged target molecules, creating a positive shift. According to Eq. (1.1), the left branch of the transfer curve (Fig. 1b) corresponds to an increase in the density of positive charge carriers (holes), whereas the right branch indicates an increase in the density of negative charge carriers (electrons).

$$I_{DS} = g_m (V_g - V_{Dirac}) \tag{1.1}$$

where I_{DS} is drain-source current, g_m is transconductance, V_g is gate voltage and V_{Dirac} is dirac point voltage. The equation down below shows the transconductance of graphene channel FET device;

$$g_m = (\frac{W}{L})\mu C_g V_{DS} \quad (1.2)$$

where g_m is transconductance, W/L is width and length of graphene channel, μ is mobility of charges in graphene, C_g is capacitance of gate, V_{DS} is drain-source voltage. The charge neutrality point equals the minimal conductivity when the dirac point voltage exceeds the gate voltage. The bulk of charge carriers are holes if the fermi level is located in the valence band. In the opposite case, the fermi level is put in the conduction band if the gate voltage is higher than the dirac point voltage, indicating that electrons make up the bulk of the charge carriers (Figure 1.7) ((Aspermair et al., 2021; Cai et al., 2022; Hasegawa et al., 2014; B. Li et al., 2015; Turner, 2013).

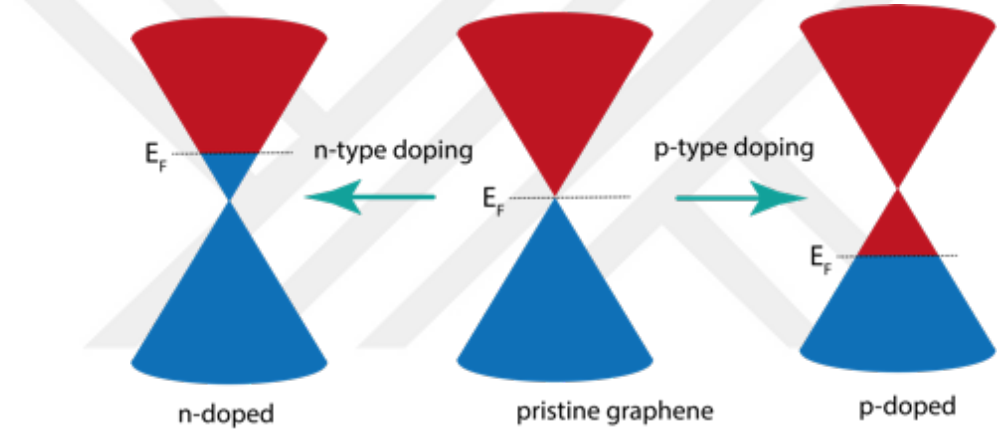

Figure 1.7. The doping of graphene.

Since biomolecules such as proteins and nucleic acids are pre-existing in biological fluids, coplanar and liquid-immersed gate configurations are greatly favored in biological GFET design as they allow sensing directly in the liquid sample without intermediate drying steps. The electrical double layer (EDL), which behaves like a much thinner dielectric layer, is what dictates the capacitance rather than where the gate electrode is located at the graphene/electrolyte interface. Therefore, Eq. (2) is used to get the final capacitance (C_{total}):

$$C_{Total} = [\frac{1}{C_q} + \frac{1}{C_{DL}}]^{-1} \text{ with } C_{DL} = e_r e_0 A/\lambda_D \quad (1.3)$$

where C_q being the quantum capacitance, C_{dl} is the double layer capacitance of the rGO/electrolyte interface, ε_r corresponds to the relative permittivity of the

electrolyte, ε_o is the vacuum permittivity, A is the area of the graphene channel, and λ_D is the Debye length. A slight change in the density of state of 2D materials like graphene, which has a high C_q, causes a significant shift in the Fermi level. Due to the fact that C_{DL} is often one order of magnitude bigger than C_q, C_q contributes the majority of the overall capacitance. The exceptional sensitivity of these GFET biosensors is due to the fact that any buildup of the analyte on the bioreceptors will result in a significant change in the Fermi level. This provides that in liquid GFET devices the applied voltage via gate is lower as ±10 V compared to back gated GFET which applied voltage is approximately ±100 V. The lower application of voltage via gate electrode as mentioned above avoiding unwanted water splitting in liquid analyte. In the next section detailed information about graphene and its derivatives were given as sensing layer.

1.3 Graphene and Its Derivatives

Because of its exceptional optical and electrical properties as well as its high surface to volume ratio, graphene (Figure 1.8), a 2D one-atom thick carbon material with a honeycomb hexagonal lattice structure, has emerged as an excellent option for biosensors. Novoselov and Geim, two scientists from Manchester University, successfully exfoliated graphene using the scotch tape method from graphite in 2004, earning them the Nobel Prize (Novoselov et al., 2004). In addition, graphene has remarkable chemical and physical qualities such high electron mobility, high transparency, high specific surface area, high mechanical strength, and ease in interacting with other biomolecules via stacking of π-π bonds. These characteristics allowed graphene to obtain major application opportunities in biology, material science, and drug delivery (Lerner et al., 2017; Peña-Bahamonde et al., 2018). Graphene has attracted significant scientific attention in bio-sensing applications ever since it was discovered in 2004 (Novoselov et al., 2004) because of its capacity to detect minute concentrations of a variety of macromolecules, such as proteins and nucleic acids, as well as different analytes and clinical infections (Andronescu & Schuhmann, 2017; Bobrinetskiy & Knezevic, 2018; Rodrigues et al., 2022; X. Wu et al., 2018). All of these properties that graphene has provided to scientist's usage of this material in biosensor devices.

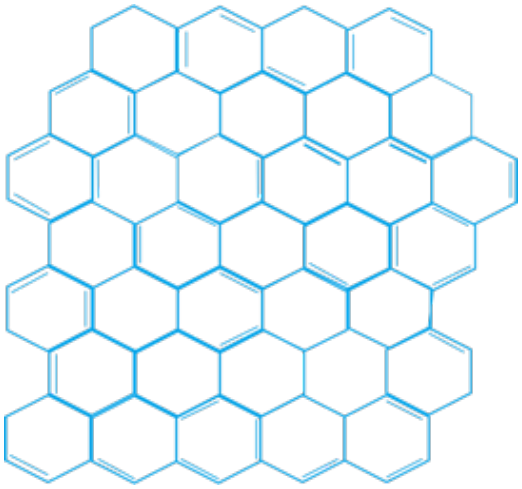

Figure 1.8. The chemical structure of graphene.

There are two approaches of while obtaining graphene as top-down and bottom up. In top-down production method, generally as starting material graphite is preferred for exfoliation. On the other hand, in bottom up approach the one has to use carbon precursors for graphene growth on substrate. The brief information about are various exfoliation methods for graphene as given below;

- Mechanical exfoliation: This method is used for obtaining monolayer graphene sheet by using mechanical methods. For example, the scotch tape is used to obtain graphene layer by peeling of graphite material. However, this method is not suitable for mass production. And also, distinguishing of proper graphene layer for its usage can be difficult (Lerner et al., 2017).
- Chemical vapor deposition (CVD): One of the bottom-up technique of producing graphene, in the process of producing graphene is done under high temperatures (1000ºC). As precursor the gas phase of the methane is used as carbon source and other carrier gasses as Hydrogen and Nitrogen. During process, the metal foils such as Cu or Ni is used as substrate. The production of graphene with this method is challenging due to controllability of graphene growth. In addition, the large-scale production of this method is very limited. Literature studies showed that mostly graphene production is done on Cu foil with dimensions of 2 mm × 2 mm, 3 mm × 3 mm, 5 mm ×5 mm (Lerner et al., 2017; Szunerits et al., 2023).
- Thermal Growth: This method belongs to bottom-up techniques that uses SiC (silicon carbide) material while producing graphene. The advantage of this technique provides the usage of graphene in electronic equipment. However,

high quality functionalized graphene has significant unwanted defects at the end of process (H. Liu, 2014).

Due to advantages that mentioned above, the graphene used in many sensor applications such as photodiodes, chemical sensors, electrochemical sensors, and FET-based sensor (Kong et al., 2016; Myung et al., 2011; Zhou et al., 2022). Also, derivatives of graphene also great consideration for the purpose of application in sensor technologies. Graphene has alternatives as graphene oxide and reduced graphene oxide. In the next section, the information about is provided for graphene oxide and then reduced graphene oxide.

1.3.1 Graphene Oxide (GO)

Graphite is oxidized and exfoliated to produce graphene oxide (GO), a two-dimensional (2D) nanomaterial made up of single-layer sheets of sp^2 hybridized carbons, sites of sp^3 hybridized carbons, and oxygenated groups (Figure 1.9). Due to its oxygen-containing functionalities, including as hydroxyl, carboxyl, carbonyl, epoxide, and quinone groups, GO is extremely dispersible in water and polar organic solvents (Palas et al., 2019; Paulmurugan et al., n.d.). GO also shows the properties as large surface area, straightforward modification, chemical stability, good biocompatibility etc.

The 2D planar structure, huge surface area, simple modification, chemical stability, strong biocompatibility, and great mechanical strength are further outstanding and distinctive qualities that GO demonstrates (Jeong et al., 2016; Yoo et al., 2012). Specifically, GO may strongly interact with a wide range of small molecules and macromolecules (such as medicines, proteins, metals, and biomolecules) via π-π stacking, covalent bonding, hydrophobic interactions, electrostatic forces, and hydrogen bonding (B. Li et al., 2015; Y. Li et al., 2014; Science & Lu, 2018; Zuñiga et al., 2022). However, the studies also show that for the application in FET-based biosensor devices, to immobilize the biomarker materials linker has to be used (Hao et al., 2020). For the purpose, alternative to GO, rGO has emerged for the FET-based biosensors.

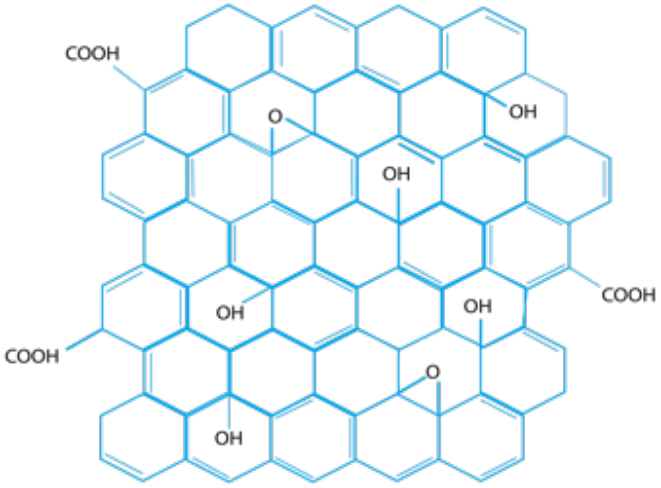

Figure 1.9. The chemical structure of GO.

1.3.2 Reduced Graphene Oxide (rGO)

As 2D material graphene alternative, rGO has oxygen-containing functional groups such as hydroxyl, carboxy etc. On the other hand, rGO has fewer oxygen-containing functional groups than graphene oxide (Figure 1.10). It is made by chemically oxidizing natural graphite, and it may be utilized for sensors, batteries, and the adsorption of different compounds (Abdolhosseinzadeh et al., 2015; Ickecan et al., 2017; Y. Wang et al., 2018). Due to reduced graphene oxide's huge surface area and excellent efficacy in immobilizing biomolecules, it has been widely utilized in the biosensor industry (Bonavolontà et al., 2021; Hasegawa et al., 2014).

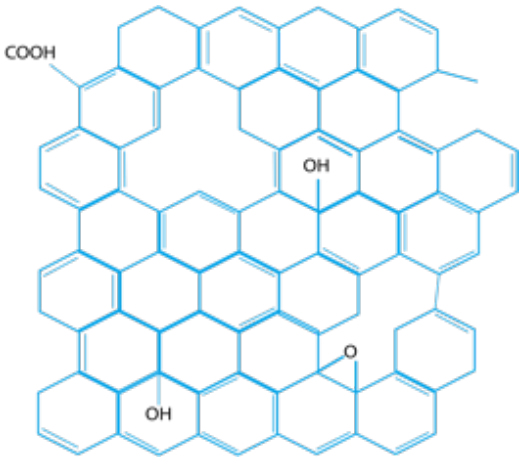

Figure 1.10. The chemical structure of rGO.

For the next generation of point-of-care biosensors and energy storage devices, rGO has a variety of oxygen vacancies that may be modified with other nanomaterials or biological molecules to further enhance their chemical and physical characteristics (Jin et al., 2019). Generally, without the use of coupling agents, the majority of biomolecules may be physically adsorbed on the surface of rGO nanocomposites. This is the quickest and easiest way for creating rGO nanocomposites with biomolecule functionality (Taniselass et al., 2019). The interactions between biomolecules and rGO nanocomposites are significantly influenced by the forces between them, including π–π stacking, electrostatic interactions, hydrogen bonds, and hydrophobic interactions. To further functionalize rGO nanocomposites, metals, metal oxide nanoparticles, and polymeric materials can be utilized as linkers to form non-covalent bonds (Mohammadnejad, Basirhaghighi, Yazdian, Pourmadadi, Shabani Shayeh C, et al., 2023; Park et al., 2020; Yamada et al., 2019). In addition to mediating a stable link between the biomolecules and rGO nanocomposites, these two-part applications also improve and magnify the transmission of sensing signals. For the synthesis of rGO for biosensor application, various methods can be used which are thermal treatment, chemical reduction etc. Most common used method is synthesis of rGO is reduction of GO. The GO can be converted rGO with heat treatment or chemical treatment. The heat treatment can be done with furnaces one of the easiest methods under gas ambient (Tu et al., 2015). The chemical reduction process for rGO can be done using chemicals like hydrazine, L-ascorbic acid, green reduction agent etc. The hydrazine is the most used chemical for reduction of GO. However, hydrazine is toxic material chemically (Habte & Ayele, 2019). Instead of using hydrazine, the L-Ascorbic acid is getting attention (Andrijanto et al., 2016; Tas et al., 2019). In the conducted study, the rGO is preferred for sensing area in FET-based biosensor devices.

1.4 Lymphoma Cancer

According to World Health Organization (WHO) projections, the number of cancer patients will rise to 24 million, and the number of cancer deaths would climb to 14.5 million (Bai et al., 2020). The four malignancies that have the greatest global effect are colon, breast, pancreatic, and lung cancer. (Sharifianjazi et al., 2022). However, the lymphoma cancer, which will cause close to 300.000 deaths

worldwide in 2020, is also a major threat to people's health (Ferlay J et al., 2020; GLOBOCAN, 2020). More than a million individuals are affected by lymphoma, a disease of the lymphatic system (B and T cells) that ranks fifth among all cancer types in the globe (Fernandez-Mercado et al., 2015). Lymphomas, which are conventionally divided into Hodgkin and non-Hodgkin lymphomas (NHL), are a very varied category of tumors that differ in their appearance, prognosis, and pathophysiology (Figure 1.11). According to the most recent WHO classification, there are more than 100 different forms of lymphoma, the majority of which are B-cell derived (Solé et al., 2017). Diffuse large B-cell lymphoma (DLBCL) and follicular lymphoma are the two most prevalent kinds of NHL, accounting for more than 60% of all cases (Bedewy et al., 2017). Also, the occurrence of NHL in Turkey reached to 233834 and expected to increase to 392383 cases by 2040 (Figure 1.12) (GLOBOCAN, 2020).

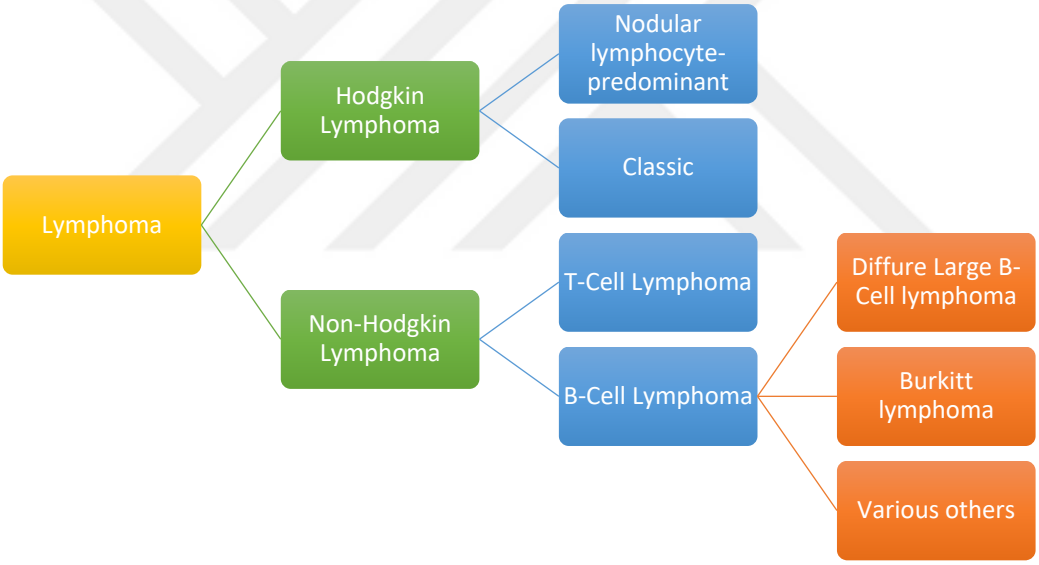

Figure 1.11. Lymphoma Cancer Types.

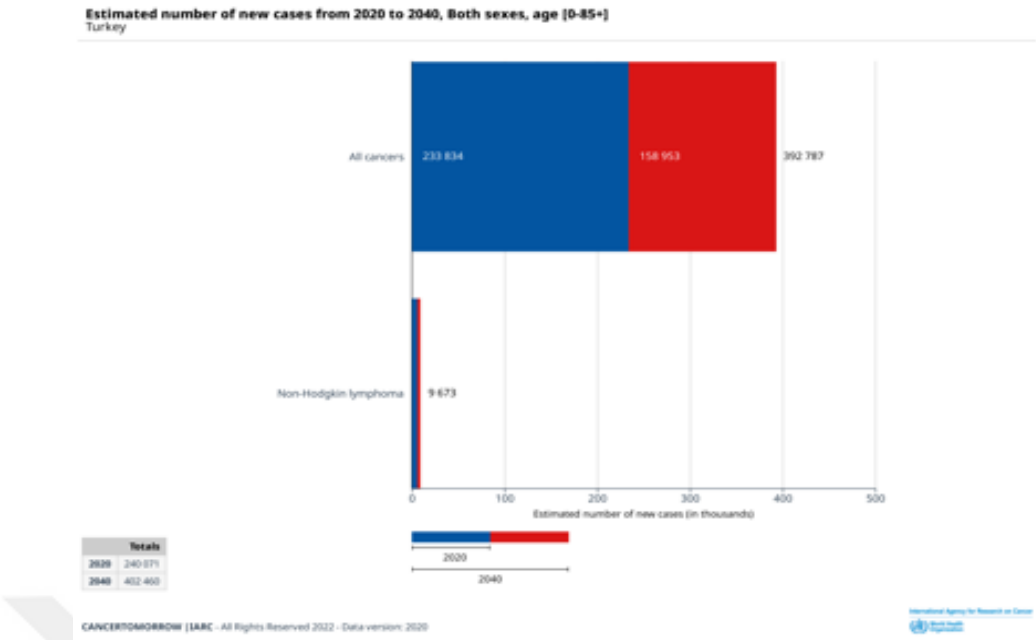

Figure 1.12. The Current and Future prospects of Non-Hodgkin Lymphoma cancer in Turkey (2020-2040).

Chemotherapy, surgery, and radiation are examples of general cancer treatment methods that are typically used to identify the cancer cells when they are still in the early stages to prevent caused by it (Bohunicky & Mousa, 2011). Therefore, a fast cancer diagnosis is essential for choosing an efficient cancer therapy. However, conventional diagnostic methods including computed tomography (CT), X-rays, and magnetic resonance imaging (MRI) are pricey and typically have a significant waiting period (Aamri et al., n.d.; Chandra & Nee, n.d.; Mohanty et al., 2012; Science & Lu, 2018). Furthermore, the success of any early cancer detection is far from certain because conventional diagnostic methods need several million cells for an appropriate clinical diagnosis. A sensitive sensor must be able to identify a limited number of samples with great sensitivity and selectivity in order to successfully diagnose cancer early and treat it effectively (Bhalla et al., 2016b; De Micheli et al., 2012; Fales, 2014). The last trend of determination of early diagnosis of cancer is liquid biopsy. In particular, biological fluids are sampled to keep track of the quantity of cancer biomarkers present in the selected medium. To date, peripheral blood and blood-derived substances like plasma and serum have received the greatest attention as liquid biopsy medium (Bellassai & Spoto, 2016). With the advantages provided the liquid biopsy, the detection of diseases can be operated quickly and

harmless. Circulating tumor cells (CTCs) have been the subject of the bulk of liquid biopsy research to far, but since these cells are relatively uncommon, sensitive collection and enrichment techniques are needed. Circulating (or cell-free) nucleic acids (cf-DNA/RNA) are increasingly being the focus of liquid biopsy research due to their ease of collection and analysis. Particular attention has been paid to circulating cell-free microRNAs (cf-miRNAs) as part of liquid biopsy (Larrea et al., 2016). The detailed information about miRNAs is given in Section 1.5.

1.5 miRNAs as Cancer Biomarkers

A common component of viruses, plants, and mammals, miRNA is a small, non-coding RNA molecule that may control mRNA expression at the post-transcriptional stage. miRNAs are important for a variety of physiological and pathological processes, and altered miRNA expression is associated with the onset and progression of cancer (Balacescu et al., 2019). It does not encode functional proteins, but by complimentary pairing with the target mRNA it can degrade or limit protein translation, which in turn inhibits the expression of a certain gene (Wen et al., 2021). The miRNAs are small (18-25 bp) and single stranded RNAs sequences that can be found in human blood mechanism (47). The regulation of gene expression by miRNAs has an influence on a number of physiological and metabolic processes (Drees & Pegtel, 2020). The literature studies have been showed that because of expression in blood, the miRNAs can be useful forerunner detection marker. Due to this advantage, the miRNAs can be used in early diagnosis (Saliminejad et al., 2019; Solé et al., 2018). Reverse transcriptase polymerase chain reaction (RT-PCR), Northern blot, and microarray were the main techniques used in the early miRNA test (Y. X. Chen et al., 2018). These methods describe the miRNAs, but they may be used by trained personnel in medical facilities or specialized labs (Yan et al., 2017). Currently, more than 1000 human miRNAs have been discovered, and these molecules can target more than 30% of the human genome (Mohammadnejad, Basirhaghighi, Yazdian, Pourmadadi, shayeh, et al., 2023). Some of the discover miRNAs that related specific cancer types as miR-145, miR-185, and miR-148 for prostate cancer (Coradduzza et al., 2022), miRNA1268b for lung cancer (Asakura et al., 2020), miRNA-141 for ovarian cancer (Negahdary & Angnes, n.d.) and miRNA-155 for lymphoma cancer (Lawrie, 2013). In the study of Zhong et al, the test results revealed that the miRNA-155 is the over expressed

among 90 patients and control group (ZHONG et al., 2012). The study of Hamed et al also revealed that 32 patients in the study showed miRNA-155 expression that related with lymphoma cancer (Hamed et al., 2021). Also, 84 patient and 15 control group revealed that the miRNA-155 expression carry prognostic value for lymphoma cancer (Bedewy et al., 2017). All these results offer experimental support for the use of miR-155 as a possible blood-based biomarker for the initiation and progression of lymphoma cancer (Due et al., 2016; Eis et al., 2005; Fernandez-Mercado et al., 2015; Lawrie, 2013; Solé et al., 2018; ZHONG et al., 2012).

2. AIM AND SCOPE OF THE STUDY

While the basis of the current study is the production and application of biosensors for the early diagnosis of lymphoma cancer, the following objectives were carried out one by one within the scope of the study towards the main purpose of the study.

1. **The synthesis of Reduced Graphene oxide;** the synthesis of rGO material is important for FET based biosensor devices. As a final product rGO-FET structure contains sensing area which in our case is reduced graphene oxide.
2. **The fabrication of Field Effect Transistor with Reduced Graphene Oxide;** The transfer of rGO to FET device is challenging issue. Also, the studies in literature shows the importance of this challenge.
3. **The investigation of rGO-FET for biosensor applications;** To examine the applicability of rGO-FET biosensor, the primary trials of rGO-FET biosensor device with solutions that contain various pH value.
4. **The miRNA detection with rGO-FET biosensor;** The miRNA-155 was preferred for early detection of Lymphoma cancer.
5. **The determination of rGO-FET biosensor for its use of early detection of lymphoma cancer and cancer metastasis;** the detection limits related with lymphoma cancer have been a huge problem from the beginning. For the purpose, the detection of the lowest limit for the cancer related miRNA-155 has been reached out.

3. MATERIALS AND METHODS

3.1 Materials

The graphite powder (<20 μm, synthetic), Sulfuric Acid (96%, Suprapure), Potassium Permanganate, Hydrogen peroxide (Suprapure), L-ascorbic acid (ACS reagent) were purchased from Sigma-Aldrich (Merck Company). mi-RNA-155 and its complementary were synthesized by Oligomer Biyoteknoloji A.Ş. Company. The Phosphate Buffered Saline (PBS) solution was prepared as 10 mM with 7.4 pH in Assoc. Prof. Dr. Ercan Selçuk Ünlü's laboratory.

3.2 The Synthesis of Reduced Graphene Oxide (rGO)

The generally utilized Hummer's Method was employed to the large - scale production of graphene oxide (Abdolhosseinzadeh et al., 2015). Firstly, 1g of graphite was put into 50 mL H_2SO_4. The mixture was put onto magnetic stirrer at 600 rpm. After a while, 3 g of potassium permanganate was added to mixture slowly. The mixture was stirred for 3 hours at 600 rpm. At this process, the temperature of mixture was maintained as <10°C. After 3 hours of stirring, 50 mL DI water was slowly added to mixture and the color of mixture was turned to brownish color. Afterwards, 100 mL more DI water was added to mixture and stirring was continued for 1 hour. To stop the reaction in mixture, 5 mL of hydrogen peroxide was added to mixture. The neutralization process was done by filtering mixture with blue band filter paper. The mixture was washed with DI water. After, the synthesize graphene oxide was left to dry overnight at room temperature.

The synthesized graphene oxide was turned into reduced graphene oxide by chemical reduction process. For the reduction process, 1 mg of graphene oxide and 2 mg of L-ascorbic acid and 50 mL of DI water were mixtured and stirred at 900 rpm for a day. Afterwards, the mixture was filtered and washed with DI water. The washed mixture was left to dry overnight at room temperature. Consequently, the synthesis of reduced graphene oxide was completed. The characterization of synthesized graphite, graphene oxide and reduced graphene have been done by inspecting Raman spectroscopy, X-Ray Diffraction Spectroscopy, Fourier Transform Infrared (FTIR) spectroscopy, and Transmission Emission Microscopy TEM).

3.3 Fabrication of Graphene FET Sensor

The detailed fabrication procedure of Graphene FET sensor was explained in details in below.

3.3.1 RCA Cleaning of Silicon Wafers

One of the main issues in the production of micro- and nano-electronic sensors is contamination. The sensor's performance will significantly decline as a result of contamination. To get over this disadvantage, Radio Corporation of America (RCA)'s cleaning method was used on n-type (100) silicon wafers with 2-4 resistance. The whole cleaning process were done in wet benches in 100-1000 cleanroom of Bolu Abant İzzet Baysal University Nuclear Radiation Detectors Applications and Research Center (NÜRDAM). The detailed information of this process as follows;

1. **Organic Cleaning:** The organic impurities that may be present on silicon wafers were entirely eliminated in this process. Hydrogen peroxide (H2O2), DI water (18 M), and ammonia solution (NH4OH) were produced in a specific ratio and heated to 55 °C. After being in this solution for 15 minutes, the silicon wafers underwent 10 cycles of DI water rinsing.
2. **Ionic Cleaning:** For this step, the heavy ions (e.g., Fe+, Mg+, Mn+) were completely removed on silicon wafers. At first, the mixture contains Hydrochloric acid (HCl), hydrogen peroxide (H_2O_2) and DI water were prepared at certain volumes. After that, silicon wafers were put into mixture for 15 minutes. Next step was rinsing silicon wafers with DI water for 10 cycles.
3. **Natural Oxide Cleaning:** The natural field oxide may grow on the silicon wafers unintentionally. To exterminate this oxide layer, this process has been done with dilute Hydrofluoric (HF) solution. The mixture was prepared with ratio of 50:1. The silicon wafers put into dilute HF solution for 20 seconds and rinsed with DI water for 10 cycles.

3.3.2 The Lithography Process of Ti/Au Contact Structure

Silicon wafers were placed in SiO_2 growth diffusion furnaces prior to the lithography process. By wet oxidation at 1100°C in diffusion furnaces, SiO_2 was grown. The structure of SiO_2/n-Si samples was given in Figure 3.1. Using a spectroscopic reflectometer, the thickness of SiO_2 was evaluated to be 300 nm.

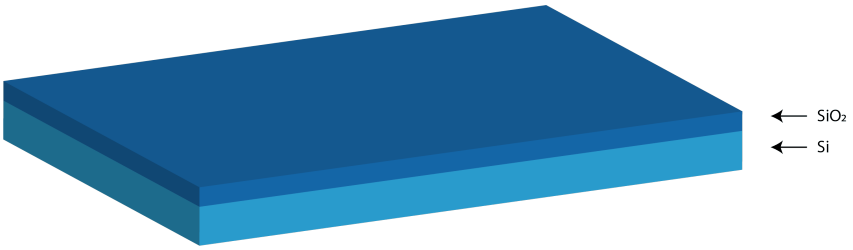

Figure 3.1. SiO_2 grown sample's structure.

The samples were coated with titanium using electron beam devices to create metal contact points. Ti was coated to promote adhesion prior to the gold electrode coating. Deposition of gold came after Ti deposition. The thermal deposition feature of the electron beam (e-beam) device was used for the gold electrode deposition. The thicknesses of Ti/Au contact points were determined as 5 nm/50 nm with spectroscopic.

For the lithography process, samples were coated with positive photoresist by using spin coating system. After coating of photoresist, the soft bake process has been done on hot plate for 50 seconds. The mask was applied with mask aligner systems. The mask design was illustrated in Figure. After applying mask, the wafers were put into developer solution for 50 seconds and then washed and dried. The hard bake procedure was done for 210 second on hot plate. After this step, the etching process has been done with Aqua Regia solution. Next, the wafers were put into remover solution to remove photoresist. The final structure was given in Picture 3.1.

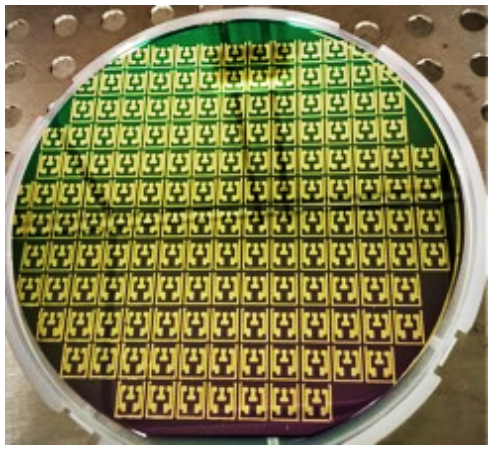

Picture 3.1. The FET structures after completion of lithography steps.

3.3.3 The Coating of Reduced Graphene Oxide on FET Structure

The reduced graphene oxide dispersion was made before applying the coating. Reduced graphene oxide was dispersed at a concentration of 10 mg/mL in an ultrasonic bath to ensure excellent dispersion. Before coating of reduced graphene oxide, the samples were covered with polyimide capton tape to prevent spreading the dispersion to other areas (Picture 3.2). Afterwards, the samples were put into plastic container for coating and placed in ultrasonic bath (Picture 3.3). The reduced graphene oxide dispersion pipetted with micropipette as 5 µL and drop casting of dispersion was done. The samples were kept until the dispersion was dry enough. Next, the samples taken out plastic container and put onto hot plate for complete dryness. The annealing step of samples were done by heating that starts from 50°C until 100°C for every in 3 minutes (Picture 3.4) (Gürer et al., 2022). Consequently, the fabrication of rGO-FET biosensor was completed. For the coating method, the patent application has been done.

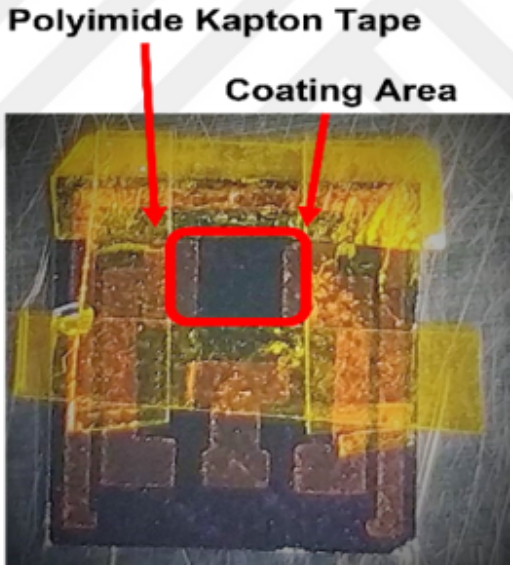

Picture 3.2. The coating area of GFETs.

Picture 3.3. The samples put into plastic container in ultrasonic bath.

Picture 3.4. The annealing step of reduced graphene oxide coated samples.

3.4 Immobilization sequences on rGO-FET biosensor

Before miRNA studies, the pH trials of rGO-FET biosensor have been completed. The various pH contained solution were dropped on rGO sensing area to prove the rGO-FET biosensor is working. The probe sequence, mi-RNA-155 sequence and non-complementary sequences were synthesized and bought from Oligomer Biyoteknoloji A.Ş. company. The sequence of miRNA-155 and probe

sequence which is complementary of miRNA-155 sequence and non-complementary of probe sequence were given in Table 3.1. The miRNA samples were kept before use in -20°C. Before functionalization of miRNAs, the GFET sensors were put onto hot plate. And then, the 5 µL pipetted samples of probe sequences were dropped onto reduced graphene oxide (Picture 3.5). Then, samples were heated to 50ºC and waited for 30 minutes for incubation of miRNA onto reduced graphene oxide. After that, to remove unbinding parts reduced graphene oxide part were washed with deionized water. The first reference measurement of rGO-FET biosensor was taken with dropping PBS solution. After that, the miRNA-155 sequence contained solution was dropped onto probe sequence immobilized rGO-FET biosensor for hybridization. The washing procedure has been applied and measurement were taken with 1×PBS solution with Keithley 4200 SCS system.

Table 3.1. The sequences of probe, miRNA-155 and non-complementary.

	Sequences (5'→ 3')
Probe	AACCCCTATCACGATTAGCATTAA
miRNA – 155	TTAATGCTAATCGTGATAGGGTT
Non-Complementary	TCTACAGTGCACGTGTCTCCAGTA

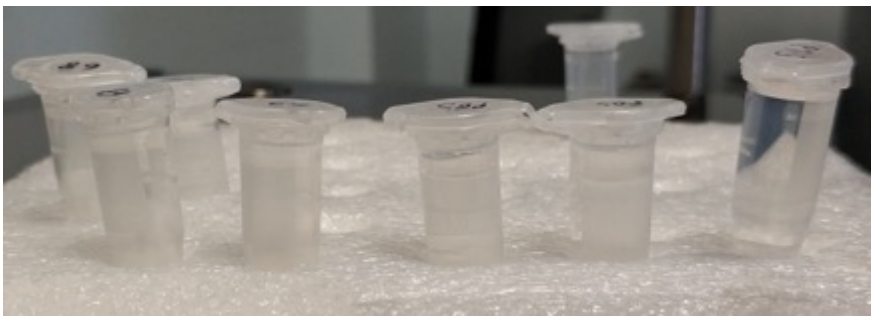

Picture 3.5. The various concentration contained sequence samples.

4. RESULTS AND DISCUSSION

4.1 Characterization of Synthesized Reduced Graphene Oxide

4.1.1 X-Ray Diffraction (XRD) Analysis

With graphite, synthesized graphene oxide, and synthesize reduced graphene oxide materials, X-Ray Diffraction (XRD) analyses have been carried out to identify the structural cellular units and also confirmation of transformation graphite to other materials. The XRD measurements has been accomplished between 5 degree and 50 degrees by Rigaku DMAX 2000/PC and Rigaku Multiflex diffractometer with CuK radiation (λ=1.54) in Bolu Abant İzzet Baysal University. The XRD spectra of graphite, graphene oxide, and reduced graphene oxide was obtained and illustrated in Figure 4.1, 4.2 and 4.3. The sharp and narrow peak was observed that belong to graphite which placed at 25.70 degree and also showed (002) plane that belong to carbon material (Figure 4.1). Also, the interlayer space (*d-spacing*) within graphite structure was found as 0.34 nm which depicts the distance between graphene layers found in graphite. As illustrated in Figure 4.2, the peak belong to carbon material was shifted to 9.82 degree after oxidation of graphite to graphene oxide by Hummer's method. This shifting in peak degree can be explained interference of oxygen-containing functional groups into graphene layers that found in graphite (Al-Mufti et al., 2022; Sieradzka et al., 2020; Tas et al., 2019). Additionally, the interference of oxygen-containing functional groups caused the increment in *d*-spacing as 0.98 nm between layers which supports the shift in peak degree. The *d*-spacing in the structure were calculated with Bragg's formula (Ickecan et al., 2017; Thakur et al., 2015).

$$d = \frac{\lambda}{2sin\theta} \tag{4.1}$$

where d is distance between layers, λ is X-Ray wavelength (0.154 nm), θ is the Bragg angle.

This result indicates successful oxidation of graphite material into graphene oxide. The same results are compatible with literature works (Abdolhosseinzadeh et al., 2015; Ickecan et al., 2017; Singh et al., 2019; Thakur et al., 2015; Verma et al., 2022). After chemical reduction with L-ascorbic acid, the reduced graphene

oxide XRD spectra was determined and illustrated in Figure 4.3. As seen in Figure 4.3, the graphitic peak with sp^2 carbon hybridization occurred at 24.93 degree and (002) plane with *d*-spacing as 0.35 nm. The sharp peak that observed in graphite structure was turned into amorphous structure and lowered intensity after chemical synthesis procedure. The causes of peak shift and reduction of *d*-spacing was caused by chemical reduction process that provides the reduction of oxygen-containing functional groups in graphene oxide. Addition of this results for reduced graphene oxide, the *d*-spacing is almost same with graphite which is proof that oxygen-containing functional groups almost removed from structure (Abdolhosseinzadeh et al., 2015; Faniyi et al., 2019; Hidayah et al., 2017; Ickecan et al., 2017; Xu et al., 2015). Additionally, rGO, a member of the hexagonal carbon family, showed a high at 44 degrees (Boukhoubza et al., 2019).

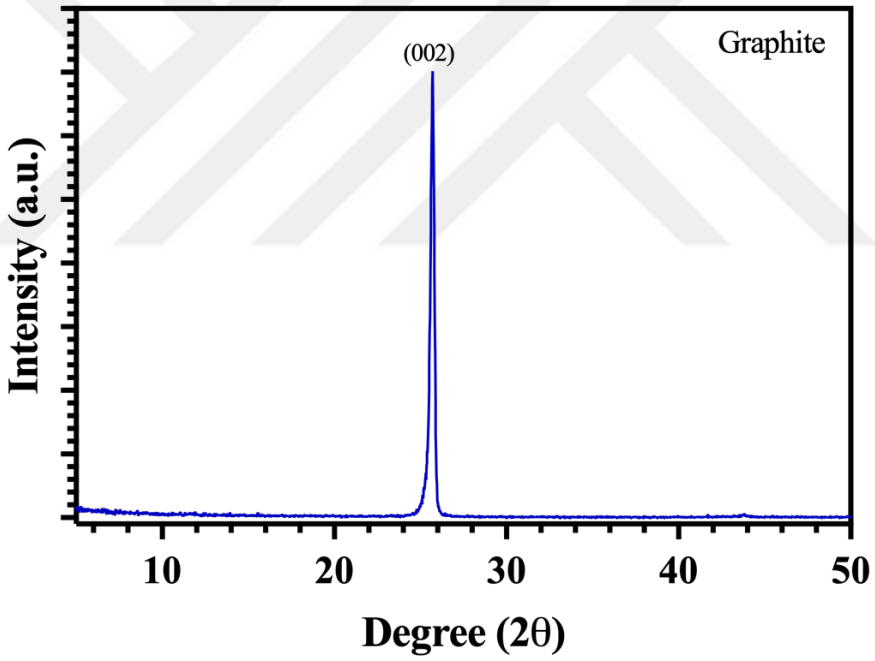

Figure 4.1. The XRD result of graphite powder.

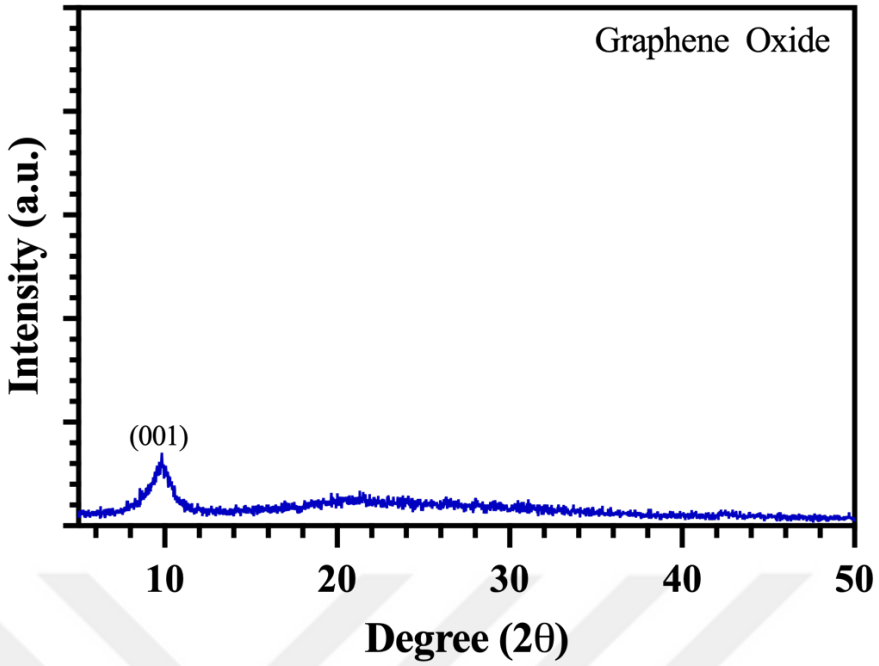

Figure 4.2. The XRD results of synthesized graphene oxide.

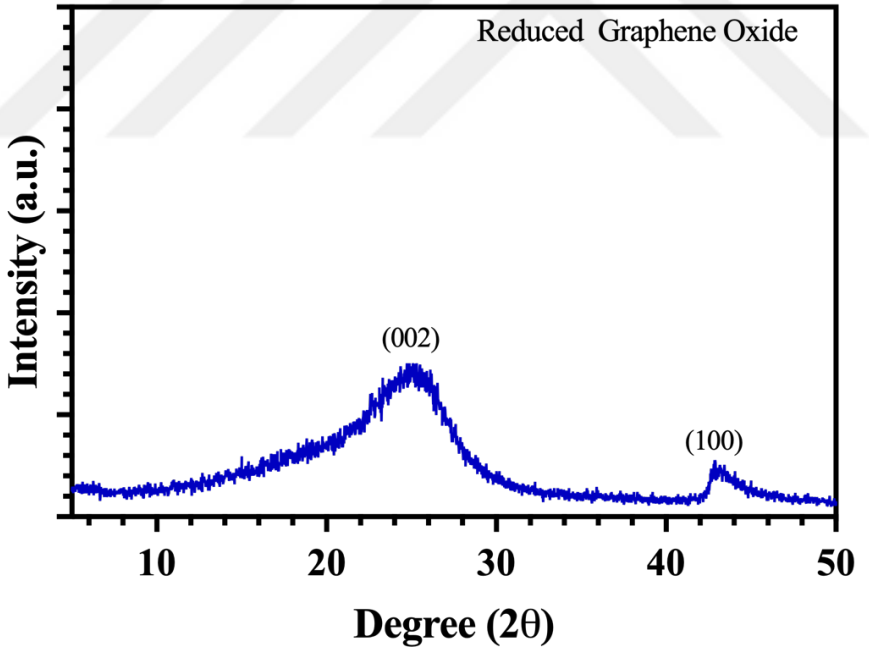

Figure 4.3. The XRD results of synthesized reduced graphene oxide.

Moreover, the average crystallite size calculations of graphite, graphene oxide and reduced graphene oxide has been calculated with the most intense peak that belong to each material. The calculation formula (Scherrer's Equation (Al-Mufti et al., 2022)) were given as below;

$$D = \frac{K\lambda}{\beta cos\theta} \tag{4.2}$$

which *D* is an average crystallite size, *K* is constant, λ (0.154 nm) is the wavelength of incident X-Rays, β is the Full Width Half Maximum (FWHM) in Radius, θ is the Bragg angle in Radius. Also, with using formula given below, the number of layers within structure was determined.

$$N = \frac{D}{d} + 1 \tag{4.3}$$

where *N* is number of layers of reduced graphene oxide, *D* is an average crystallite size, *d* is spacing between layers. The results of calculations of crystallite size and number of layers were given in Table 4.1. After calculations, it was seen that the crystallite size decreased for graphite, graphene oxide and reduced graphene oxide from 30.41 nm to 20.76 nm and 20.76 nm to 0.97 nm. The calculation result of crystallite size indicates that there was shrinking in the graphitic phase (Sharma et al., 2017). The calculations revealed the number of layers of graphite, graphene oxide and reduced graphene oxide as 88.89, 22.14 and 3.73, respectively. The graphite substance, as expected, consist of numerous layers of graphene (Al-Mufti et al., 2022). To obtain reduced graphene oxide, the oxidation of graphite has been done and the chemical reduction process was employed. After these processes, the number of layers of synthesized rGO was determined as 3.73. This result revealed that synthesized rGO consists few layers which is compatible with literature work (Kumar et al., 2021).

Table 4.1. The peak degree, measured Full Width Half Maximum (FWHM), Crystallite Size and d-spacing of graphite, graphene oxide and reduced graphene oxide.

	Degree	***FWHM***	***Crystallite Size (nm)***	***d-Spacing (nm)***	***# of Layers***
Graphite	*25.80*	*0.272*	*30.41*	*0.34*	*88.89*
GO	*9.82*	*1.94*	*20.76*	*0.90*	*22.14*
rGO	*24.93*	*8.21*	*0.97*	*0.35*	*3.73*

4.1.2 Raman Spectroscopy Analysis

The Raman spectroscopy analysis was done by inspecting over synthesized reduced graphene oxide. Raman spectroscopy measurement was taken with 532 nm laser source from METU Central Laboratory with scan range of 400 cm^{-1}-4000 cm^{-1}. The analysis results showed peak of reduced graphene oxide for *D* band at 1345 cm^{-1}, for G band at 1577 cm^{-1}, for *2D* band at 2702 cm^{-1} and for *D+D'* band at 2933 cm^{-1} (Figure 4.4 and Table 4.2). The studies showed that the "*D* band" indicates the defects in produced reduced graphene oxide and the "*G* band" indicates the recoverization of sp^2 C-C stretching vibrations in reduced graphene oxide. Besides, the existence of "2D band" gives information about number of layers within structure (Muzyka et al., 2018; J. Bin Wu et al., 2018). The ratio between intensities of D and G band (I_D/I_G) gives information about defects that found in the structure which was calculated (Table 4.2). The calculated value of I_D/I_G was determined as "*1.11*" which depicts defects was found in the rGO structure. There are different reasons of defects according to literature studies. Firstly, the defects caused in structed due to chemical processes. It is known that while converting graphite to reduced graphene oxide, the chemicals that used in process can cause defects in the structure (Owji et al., 2022; Syama & Mohanan, 2019). Secondly, the defects caused in rGO may cause by ultrasonic treatment. As mentioned in experimental part, the ultrasonic bath was used in the chemical reduction process for reduced graphene oxide. During this step, the vibration provided by ultrasonic bath can cause defects in the rGO. The works of Lee et al., Li et al. and Martinez-Pérez were also supporting the cause of defects by ultrasonic treatment (Le et al., 2019; Y. Li et al., 2013; Pérez-Martínez et al., 2016). As mentioned, one of the advantages of Raman spectroscopy is also giving information about number of layers in rGO structure. The ratio of intensities of I_{2D}/I_G provides information about numbers of layers of reduced graphene oxide (Sharma et al., 2017; J. Bin Wu et al., 2018). The ratio was determined as "*0.52*". This calculated ratio of I_{2D}/I_G depicts that the synthesized rGO contains few layers and consistent with literature (Bleu et al., 2019). In addition, the result of layer calculations is in good agreement with XRD results.

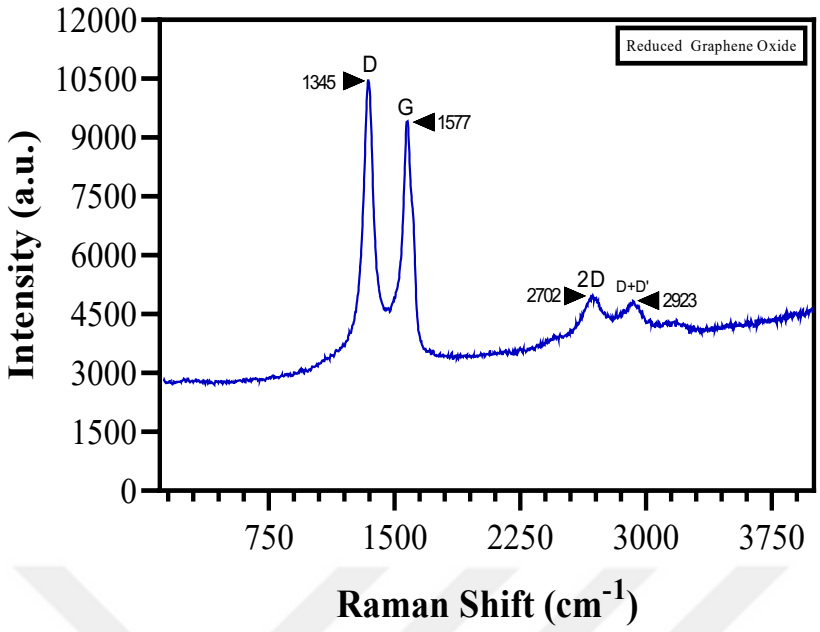

Figure 4.4. The Raman Spectroscopy of Reduced Graphene Oxide.

Table 4.2. The peak intensities of reduced graphene oxide.

Peak Name	***Raman Shift (cm^{-1})***	***Intensity***
D Band	1345	10478
G Band	1577	9429
2D Band	2702	4924
D+D' band	2923	4856

4.1.3 Fourier Transform Infrared Spectroscopy (FTIR) Analysis

The Fourier Transform Infrared Spectroscopy (FTIR) examination was carried out utilizing a Perkin Elmer Spectrum Two FTIR-ATR spectrophotometer in the Chemistry Department at Bolu Abant Izzet Baysal University to examine the bonding structure in graphite, graphene oxide, and reduced graphene oxide materials. The FTIR analysis graphics illustrated in Figure 4.5, 4.6, and 4.7. Table 4.3 also summarizes the vibration modes of that found in graphite, graphene oxide, and reduced graphene oxide. No discernible peak from graphite material was identified in the FTIR spectra shown in Figure 4.5. This finding demonstrates the material's chemical inertness which is similar in the study of Bera et al (Bera et al., 2017). After oxidation of graphite material, the graphene oxide is formed and FTIR spectra of graphene oxide is illustrated in Figure 4.6. The peaks associated with graphene oxide were identified as follows: C-O stretching vibration at 1050 cm^{-1}, C-O-C bending at 1280 cm^{-1}, O-H bending at 1347 cm^{-1}, 1557 cm^{-1}, and 1573 cm^{-1}, and C=O stretching at 1600 cm^{-1} (Andrijanto et al., 2016; X. Chen et al., 2018; Thakur et al., 2015; Verma et al., 2022). The presence of these observed peaks in the graphene oxide structure implies that oxygen-containing functional groups placed successfully between layers. Furthermore, the graphene oxide XRD spectrum complements the graphene oxide FTIR spectra. The graphene oxide was transformed to reduced graphene oxide after the L-ascorbic acid procedure and FTIR spectra of rGO was showed in Figure 4.7. From the figure, the peaks related oxygen-containing functional groups were declined and no sharp peak was observed comparing synthesized GO which depicts that removal of oxygen-containing functional groups. The similar chemical reduction procedure was used in the study of Andrijanto et al, Tas et al., and Abdolhosseinzadeh et al. and the studies concluded that the L-ascorbic acid is good reduction chemical to obtain reduced graphene oxide. In this regard, our findings are consistent with previous research papers (Abdolhosseinzadeh et al., 2015; Andrijanto et al., 2016; Tas et al., 2019). In addition, the graphs that belong to graphite and reduced graphene oxide showed similarities in structure bonding. Low intensity peaks, on the other hand, distinguish graphite from rGO. The XRD measurements also support the conclusions drawn from our FTIR spectra by means of *d*-spacing calculations.

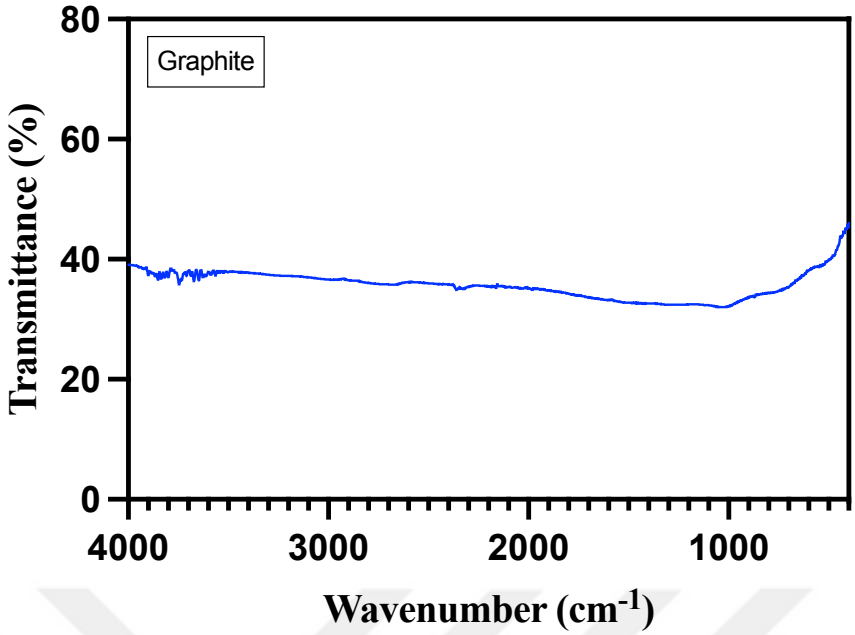

Figure 4.5. The FTIR Spectra of Graphite.

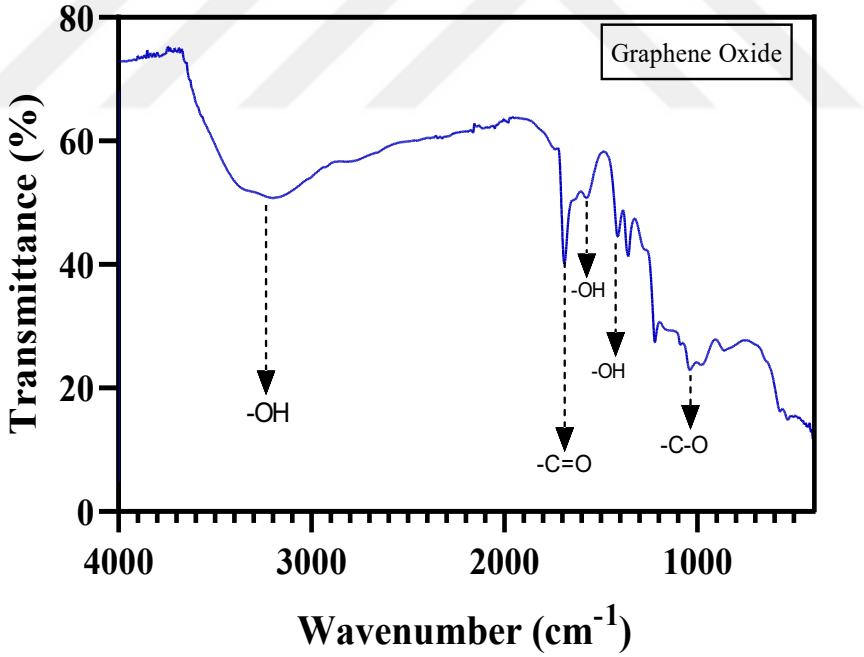

Figure 4.6. The FTIR Spectra of Graphene Oxide.

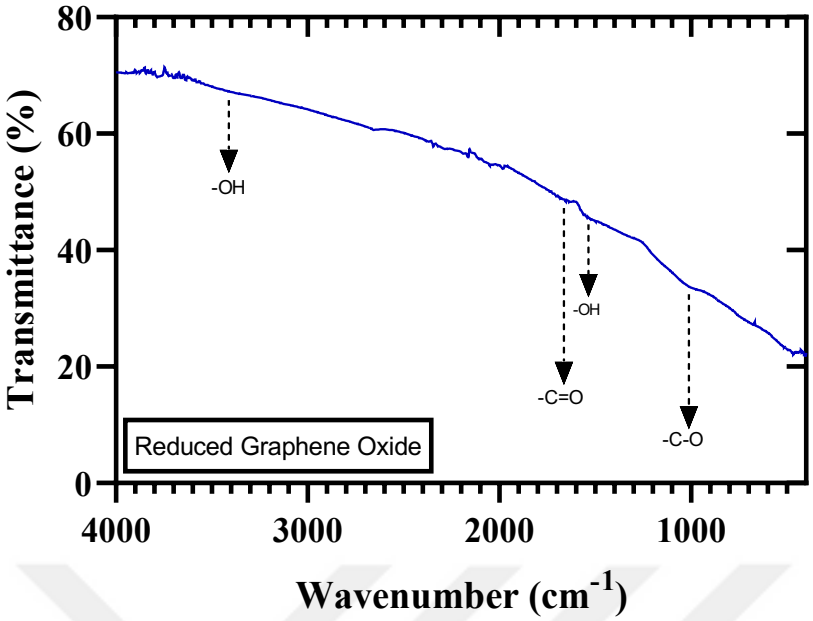

Figure 4.7. The FTIR Spectra of Reduced Graphene Oxide.

Table 4.3. The summarized vibration modes of graphene oxide.

Wavenumber range (cm^{-1})	Vibration Modes
1060	C-O
1280	C-O-C
1347	O-H
1557	O-H
1573	O-H
1600	C=O
3400	O-H

4.1.4 Transmission Emission Microscopy (TEM-R) Images

In order to examine the morphology of reduced graphene oxide material, The Transmission emission microscopy (TEM) images was taken with Jeol 2100F HRTEM with Orius SC1000 Model 832 11 Megapixel CCD camera in METU Central Laboratory R&D Training and Measurement Center. The TEM images that belong to rGO structure were given in Picture 4.1. The TEM images of rGO flakes were taken at various magnification levels which provides the visibility of layers within the rGO structure. Also, the rGO was considered as multiwall structure when inspecting TEM images. In addition, some defects such as wrinkling and folding was observed in TEM images of rGO. The similar results were found in the work of Chuah et al. that can be explained by chemical process (Chuah et al., 2020). Furthermore, the analysis of Raman spectroscopy is in good agreement with the defects/wrinkles/folding found in rGO.

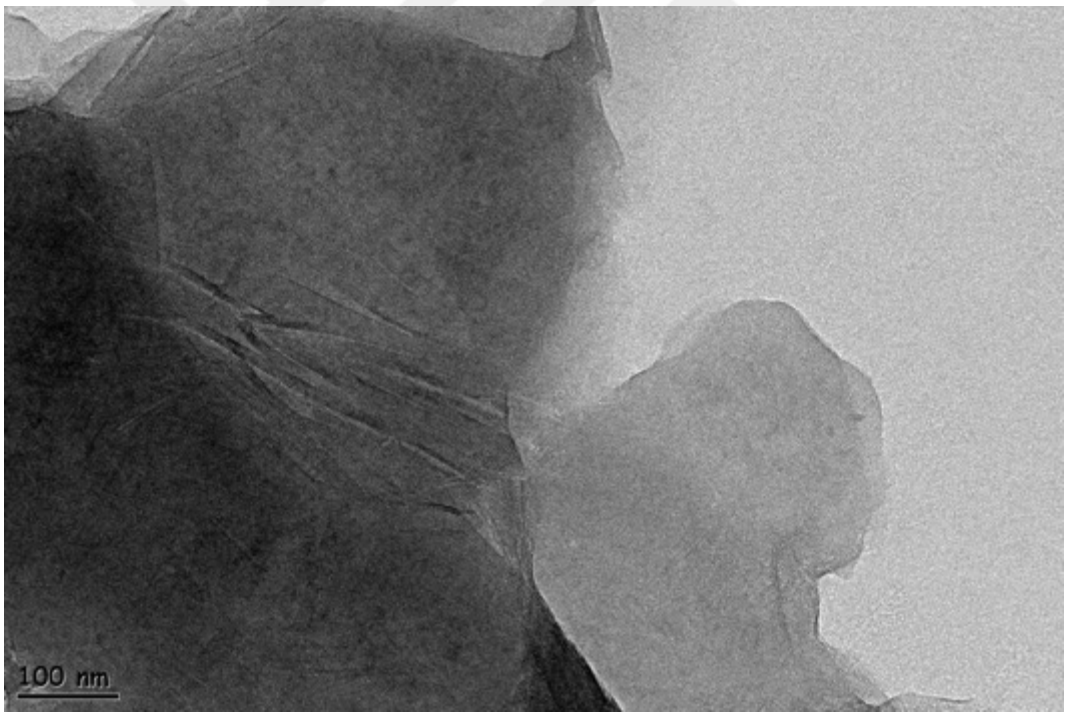

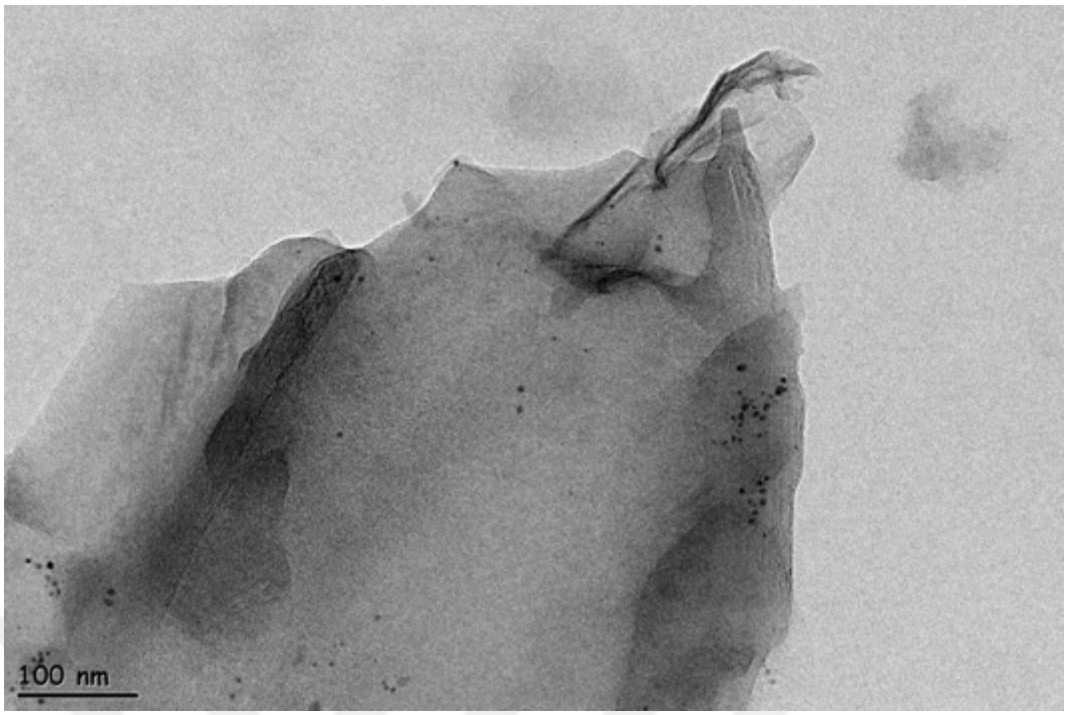
100 nm


50 nm

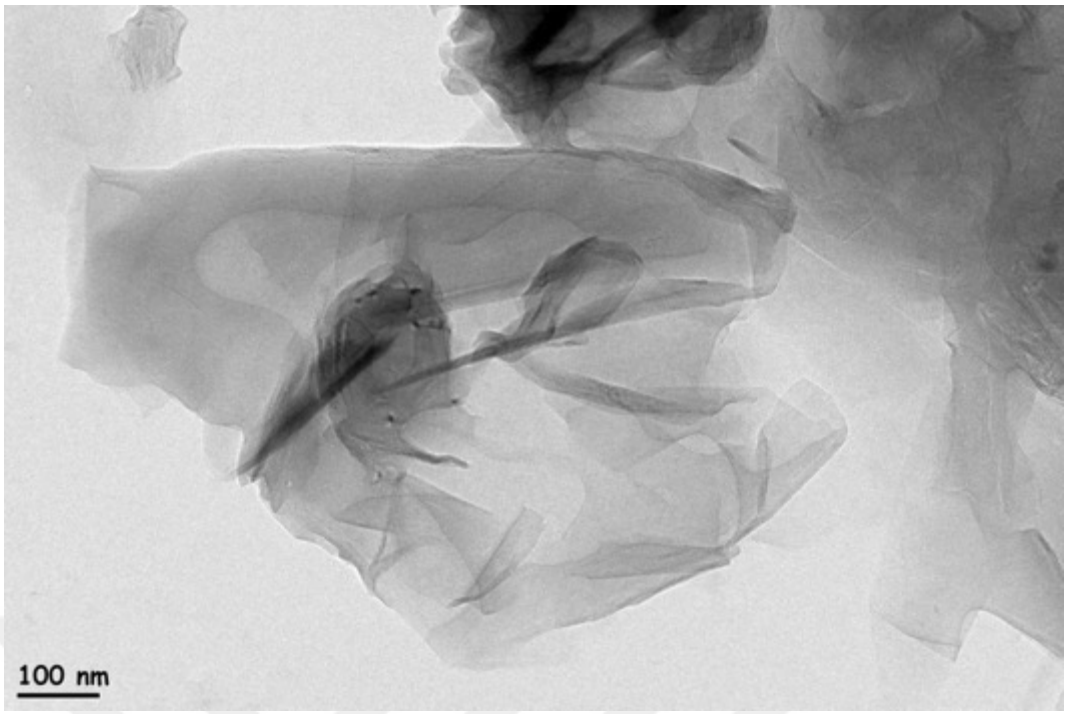

Picture 4.1. The TEM images of reduced graphene oxide material captured at different scales.

4.2 Electrical Characterization of rGO-FET Devices

The electrical characterizations of rGO-FET based devices are important for its applications to use as POC device. For the purpose, the electrical characterization of fabricated rGO-FET based biosensor has been completed with different measurements. First of all, the output characteristics of fabricated rGO-FET biosensor has been done to investigate relation between contact points and rGO structure. The output characteristics was taken while applying sweep voltage between drain and source contacts (-0.5 V – 0.5 V), the gate voltage was fixed to 0 V. Secondly, the transfer characteristics of the rGO-FET device was investigated with both pH solutions and miRNA solutions. The transfer characteristics of rGO-FET biosensor were conducted when applying sweeping voltage gate (0 V – 5V) and fixed drain voltage (0.1 V) and source is grounded. However, the voltage applied to gate differs from miRNA-155 studies for pH trials which was set between -0.5 V and 2 V. To do so, the measurement setup of rGO-FET biosensor was setup and can be seen in Figure 4.8. Keithley 4200 SCS measurement system integrated with probe station was used during measurements. The needles of probe station were connected to gate, drain and source of fabricated rGO-FET devices (Figure 4.8).

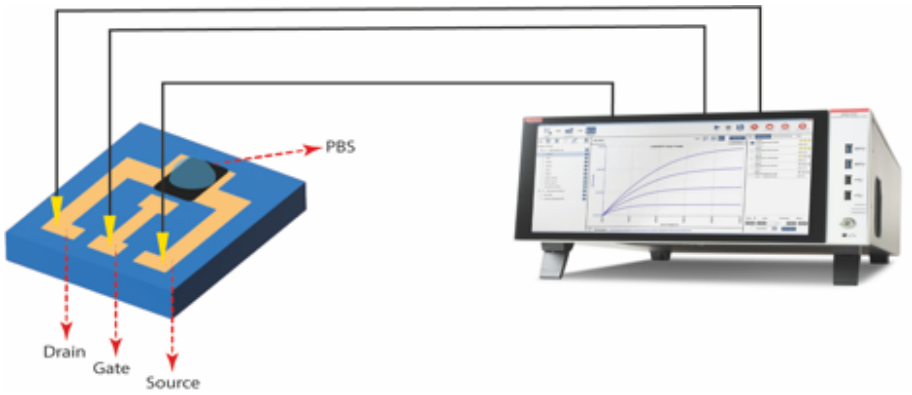

Figure 4.8. The measurement setup of rGO-FET device.

While measuring electrically of rGO-FET biosensor device, one should also consider changes during rGO surface. There are four electrical effects that effects the electrical characteristics of rGO-FET biosensor device which;

1. **Charge Transfer:** During measurements, different solutions were introduced on rGO sensing area surface and the target biomolecules in solution may

introduce different charges. These charges accumulate on the rGO sensing area and causes shift of Dirac point voltage by donating and accept charges in target biomolecules (Béraud et al., 2021; Fu et al., 2017; Kaisti, 2017; Kwong Hong Tsang et al., 2019b).

2. **Capacitance Effect:** This effect causes change in Id-Vgs graph by introducing analyte on rGO sensing area. In each measurement, the analyte media dropped onto sensing area, which causes additionally capacitance. Therefore, this also changes of I_d-V_{gs} curve (Béraud et al., 2021; Fu et al., 2017; Kaisti, 2017; Kwong Hong Tsang et al., 2019b)..
3. **Electrostatic Gating Effect:** Before the voltage applied during measurement to solution gated GFET, the analyte was dropped onto rGO sensing area. The chemical interaction occurs between analyte and rGO sensing layer and the molecules in analyte adsorbed by rGO. Therefore, the ambipolarity of the rGO changes. Due to that reason, this causes change in rGO's doping characteristics. If the positive charges accumulate by rGO, then dirac point voltage shows shift towards left side in I-V, on the contrary, if the negative charges accumulate on rGO causes right shift of Dirac point voltage (Béraud et al., 2021; Fu et al., 2017; Kaisti, 2017; Kwong Hong Tsang et al., 2019b).
4. **Charge Impurity Effect:** While transferring rGO layer on FET device, the inhomogeneous distribution of layer can occur due to drop casting method. Because of that reason, the mobility of rGO layer can also be change and there is certain change can be observed in I-V graphs. This change in I-V especially effects on current and dirac point voltage (Béraud et al., 2021; Fu et al., 2017; Kaisti, 2017).

When evaluating the electrical characteristics of the rGO-FET biosensor device should take into account above mentioned effect during sensing of any biomolecules. All of the effect cannot be neglected without each other. All the effects should be considered for the performance of the biosensor device (Béraud et al., 2021; Fu et al., 2017; Kwong Hong Tsang et al., 2019b). Besides, the electrical measurements of three different chips were performed in the transfer and output characteristics measurement processes and electrical measurements of three different chips were averaged and evaluated.

4.2.1 The pH trials with rGO-FET biosensor

The rGO-FET biosensor with various dimensions' output characteristics were measures and plotted in Figure 4.9. The output characteristics' findings demonstrated the linearity's behavior. To the best of our knowledge, the linearity of the curve I_d-V_D shows good ohmic contact occurred in structure between reduced graphene oxide and drain-source contacts. This also indicates that, the electrical conduction through source and drain flows uninterruptedly. The literature works agrees with our results (Béraud et al., 2021; Cai et al., 2022; X. Chen et al., 2018). The current of different W/L devices increases with the area covered by rGO which was expected result. The information provided by I_d-V_D suggest more current flow between source and drain. However, the increase of the dimensions of area prevents scaling for microelectronic use of devices. Thus, in the thesis study only 1.5 mm rGO-FET biosensor devices were used for further measurements.

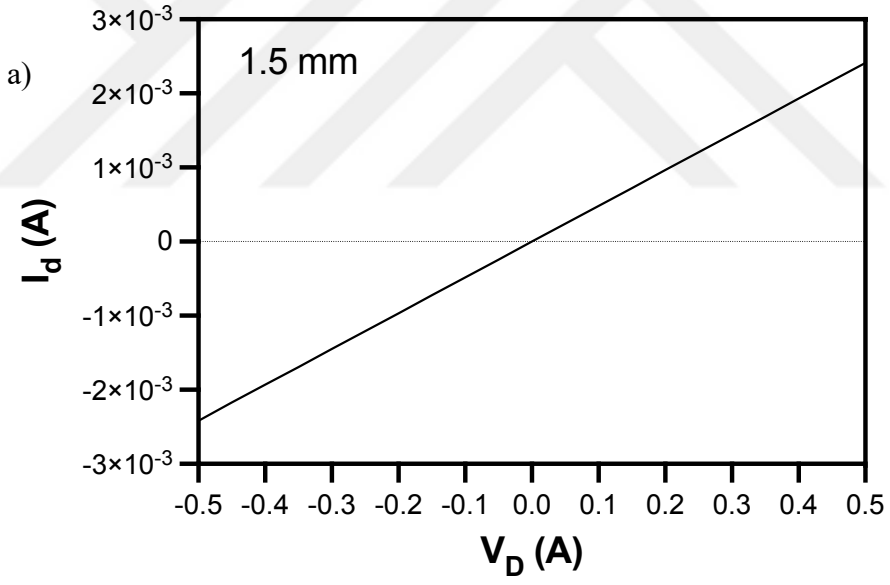

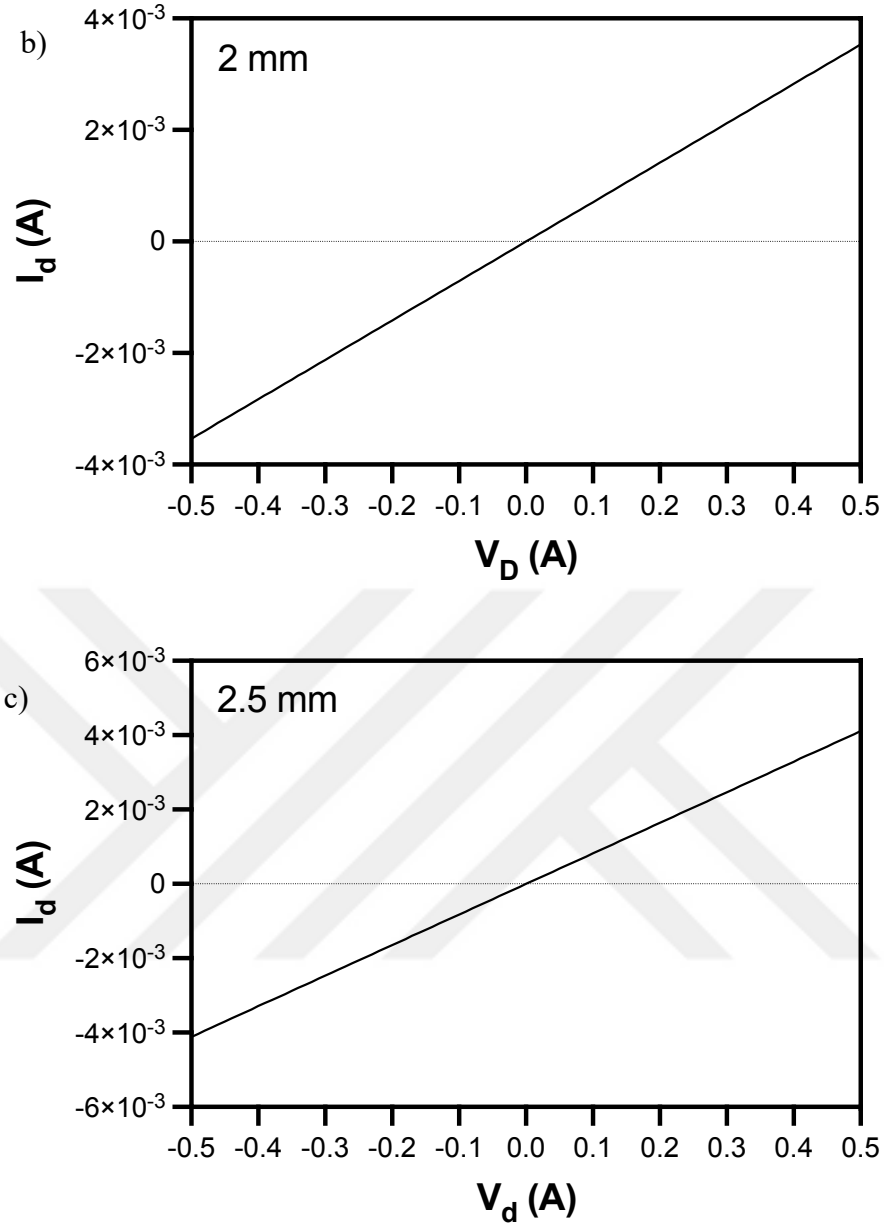

Figure 4.9. The Output curves of GFET biosensor that have widths a) 1.5 mm, b) 2 mm, and c) 2.5 mm.

For the determination of usage rGO-FET biosensor, the transfer curves of I_d-V_{gs} graph of rGO-FET device were plotted in Figure 4.10 by dropping DI water which is preferred for its chemical-free structure. The I_d-V_{gs} plot revealed the ambipolar characteristics of rGO-FET biosensor device which means the capacity of an electronic device to conduct both electrons and holes without modifying the channel doping or the contact material. From the curve, it was observed that Dirac point voltage (where electron and hole concentration is assumed equal) was at positive side which indicates the rGO layer as sensing area has unintendedly p-

doped characteristics which indicates the density of hole concentration is higher that electron concentration. The unintended p-doped characteristics of rGO can be caused chemical synthesis. It is well known that the chemical synthesis of rGO includes many chemicals, usage of chemicals can cause p-doping of rGO (Béraud et al., 2021; Hidayah et al., 2017; Thakur et al., 2015),

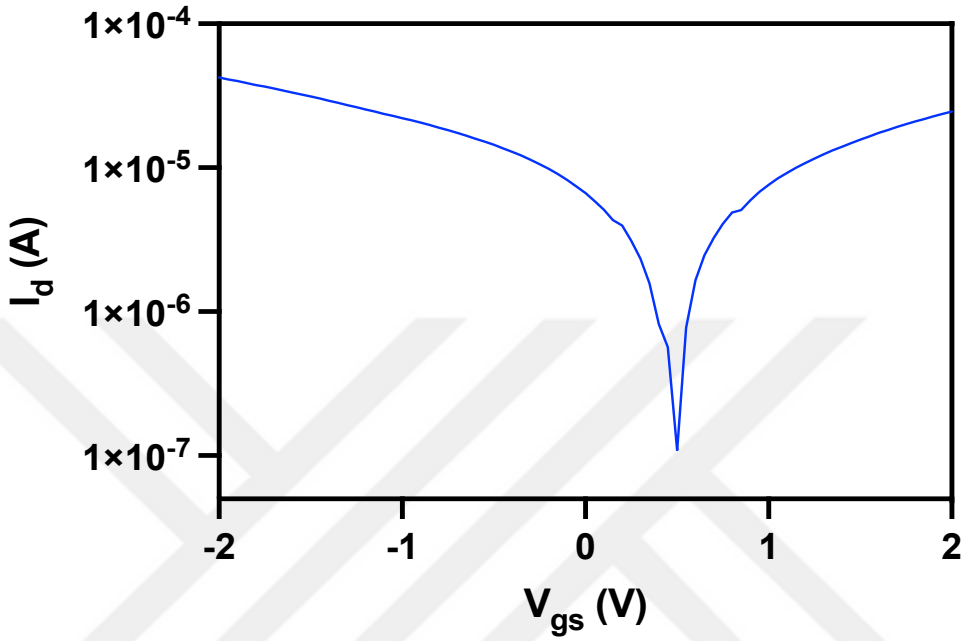

Figure 4.10. The I_d-V_{gs} graph of rGO-FET device with pH 7 DI water.

In our investigation, the solution's pH ranged from 1 to 7, and the unmodified rGO surface was in direct contact with it. As the pH raised, the dirac point voltage shifted towards right side (Figure 4.11). This change in dirac point voltage is caused by negative charge doping on reduced graphene oxide material with increasing OH ions. Additionally, we think that faulty sites in reduced graphene oxide may help with the chemisorption of the highly concentrated OH ions that are present, increasing charge tunneling onto the graphene and the efficiency of charge transfer (Campos et al., 2019; Purwidyantri et al., 2021; Vasilijević et al., 2023). The Dirac point voltage vs pH graph was illustrated in Figure 4.12. As illustrated in Figure, the linearity was observed with pH. The analysis of linear fit results indicates the R^2 value as 0.9856 which indicates the rGO-FET device can be used for biological detection.

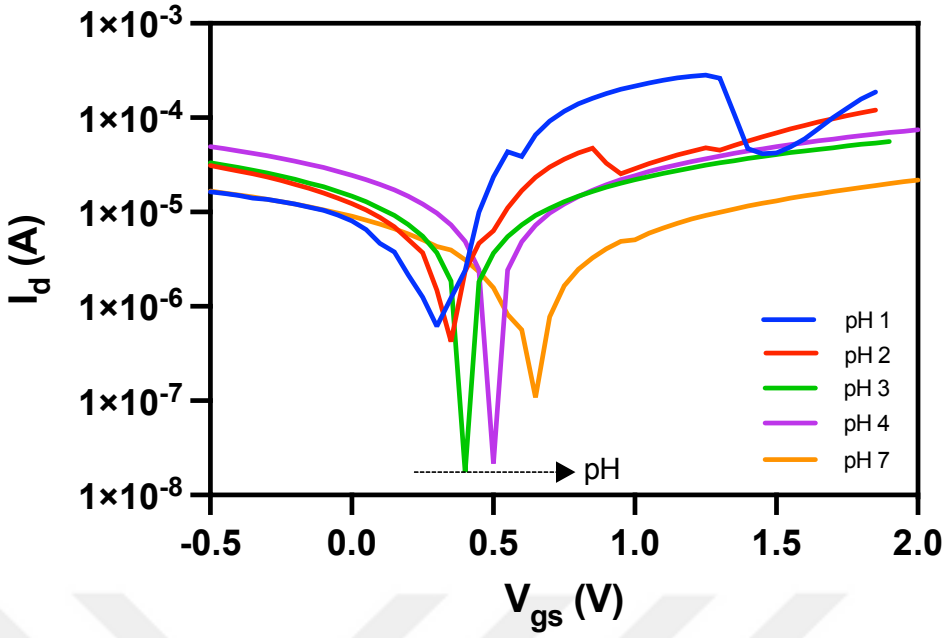

Figure 4.11. The I_d-V_{gs} graph with various pH.

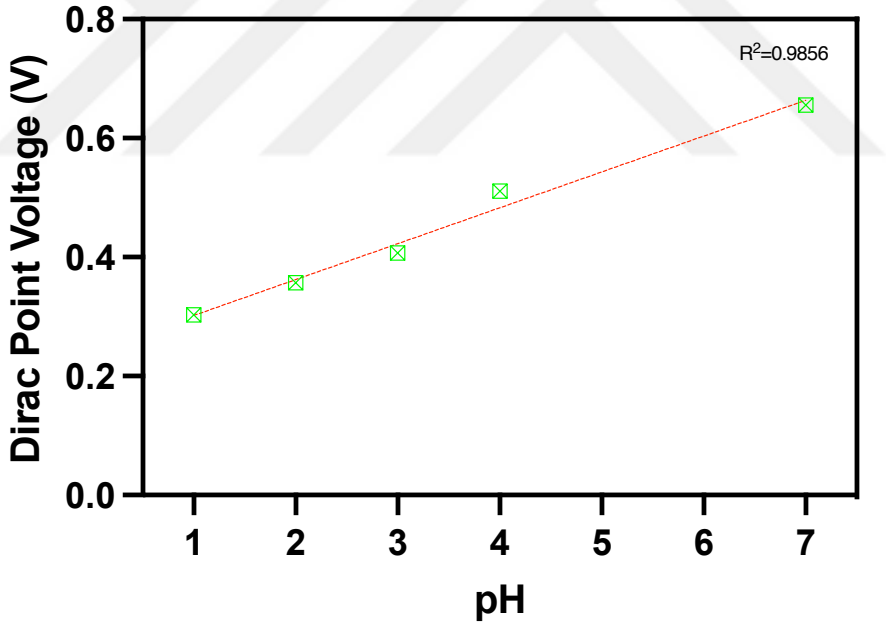

Figure 4.12. The Dirac point voltage change with pH.

4.2.2 The Electrical Characterization of miRNA-155 studies

Before examining the electrical characterizations of miRNA-155 identification by probe sequence, it is necessary to provide information about the immobilization of the sequences on rGO because rGO-FET cannot give any response without any biomaterial immobilized on rGO. From this point of view, in our study, we first tested the operability of the structure by performing pH experiments in the previous section. In the next step, we examined the electrical characterization of miRNA sequences by immobilization on rGO. Over the past years, a number of well-controlled chemical functionalization procedures have been developed that are compatible with GFETs. Immobilization studies are carried out by first integrating the counterpart of the material to be identified by a biosensor into the rGO structure. Examples of these materials include antibodies, proteins, nucleic acids. The immobilization techniques divided into two groups as covalent and non-covalent bonding (Asav et al., 2016; Fu et al., 2017; Hao et al., 2020). In covalent bonding, the biomolecules of target of interest are functionalized on rGO surface via linker materials such as amino groups (-NH2), carboxyl groups (-COOH), or epoxide groups (-O). However, this linker material causes structural change in rGO (Béraud et al., 2021). The most used linker molecules PBASE (1-Pyrene butyric acid N-hydroxysuccinimide ester) in GFET biosensors. In non-covalent bonding, mostly physical adsorption is preferred. The physical adsorption of biomolecules interact with rGO such as electrostatic forces, π-π stacking, or van der Waals interactions. In our study, immobilization of anti-miRNA-155 sequence (probe sequence in this study) structures was performed for early diagnosis of lymphoma cancer because of the properties that rGO has. The miRNAs functionalization was performed on rGO without using any other material in the conducted study (Figure 4.13). The study of Cai et al. also showed that the miRNA sequences can be directly immobilized onto rGO layers (Cai et al., 2022).

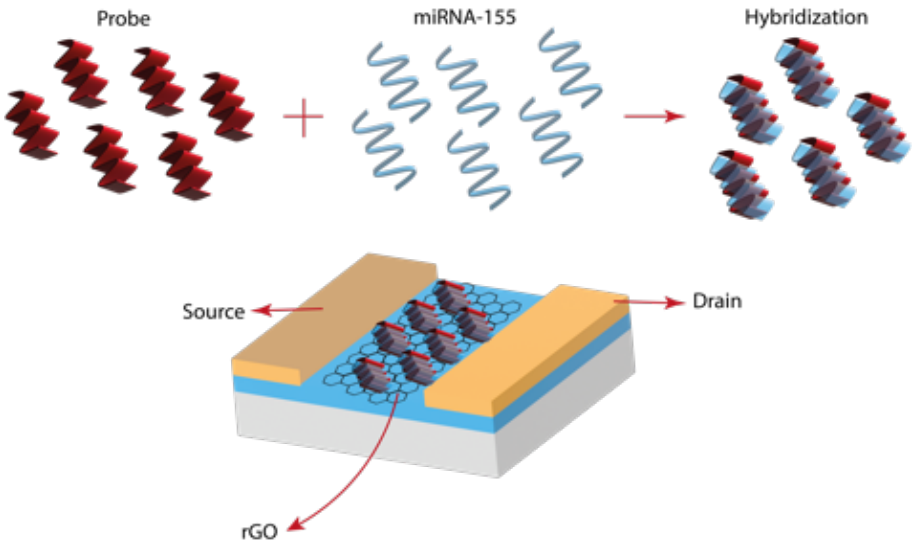

Figure 4.13. The schematic representation of hybridization of probe sequence and miRNA-155 sequence.

At the beginning, the blank measurement was taken with PBS solution with rGO-FET biosensor device. The Dirac point voltage determined as 4.3 V (Figure 4.14). And then, the probe sequence was immobilized onto surface of rGO. The I_d-V_{gs} transfer characteristics of the rGO-FET biosensor after providing hybridization of probe sequence and miRNA-155 sequence (Figure 4.15). As seen in the graph, due to hybridization between probe and miRNA-155 sequence the Dirac point shift towards to left side. The shift also provides information about the hybridization occur between probe sequence and miRNA-155 sequence. Hence, the voltage was observed before hybridization as "3.7 V", right after hybridization it was determined as "1.7 V". The shift can be explained by in some factors. First, the electrostatic effect which related with rGO structure. During experiment, the miRNA contained PBS solution were used to functionalize the rGO. In our experiments, the rGO that synthesized showed p-doped characteristics. However, the PBS solution introduce positive charges to rGO which causes shift in Dirac point voltage (Kwong Hong Tsang et al., 2019b; Santangelo MF, 2014; Velasco-Garcia & Mottram, 2003). Second is indicated that due to negative charges on miRNA-155, the electron concentration on rGO sensing area was increased and shift towards to the left was observed (Cai et al., 2022; Sreejith et al., 2023). Third is the addition of extra capacitance effect which in our study, we measured the rGO-FET biosensor device with first with PBS and then with probe sequence and with hybridization of probe and miRNA-155 sequences. Each time, we introduced

solution on rGO sensing area which may cause additional capacitance in rGO-FET biosensor device. Due to this cause, the n-doping effect caused by PBS and sequences cause shift towards to left side (Kaisti, 2017; J. Y. Kim et al., 2013; J. Li et al., 2011; Sreejith et al., 2023; Yin, 2018).

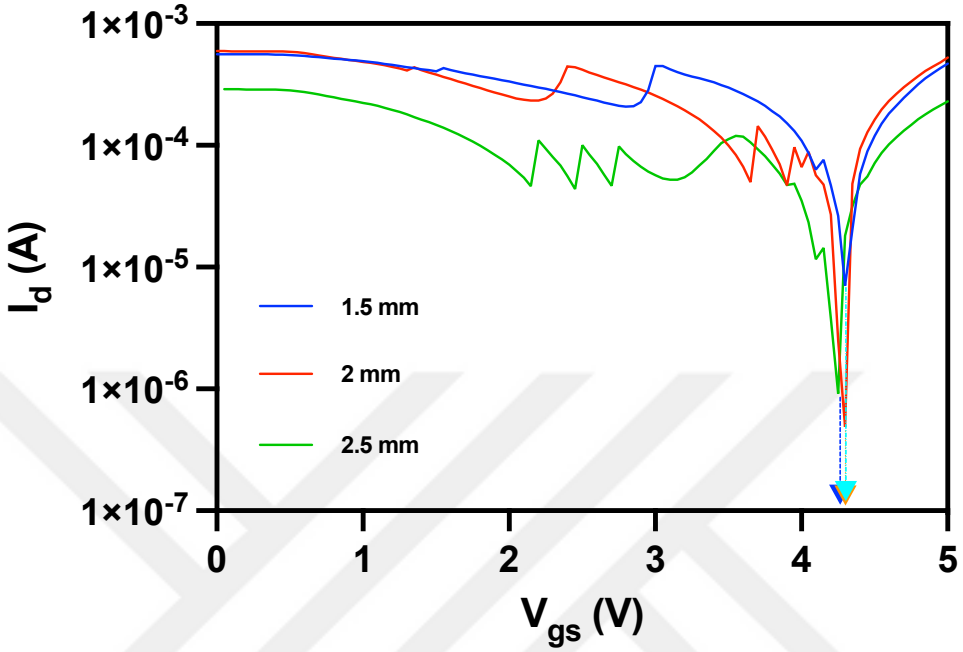

Figure 4.14. The I_d-V_{gs} graph of rGO-FET biosensor with different size.

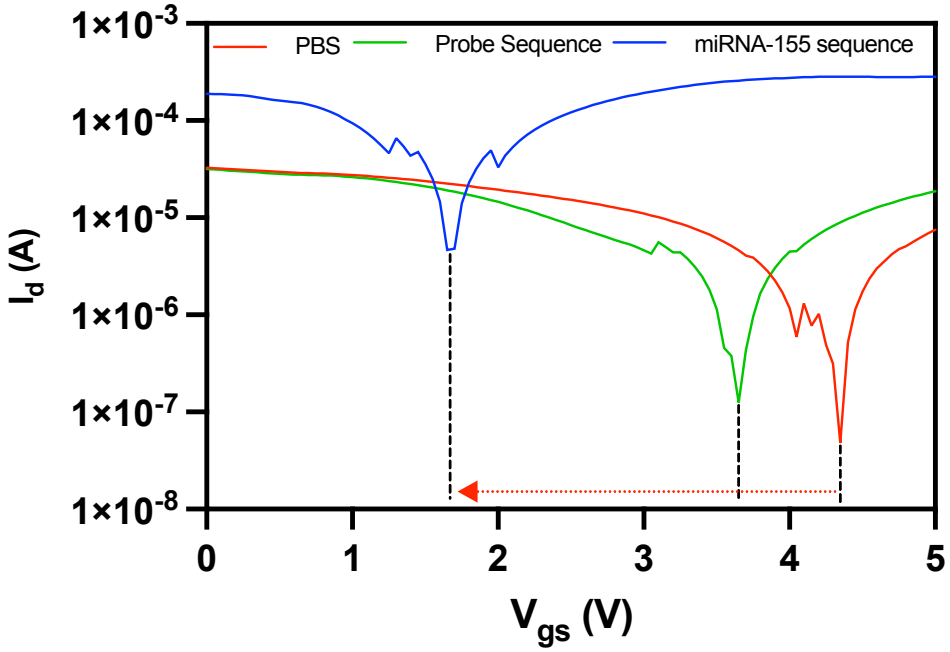

Figure 4.15. The I_d-V_{gs} graph after hybridization between probe sequence and miRNA-155 sequence.

4.2.3 Specificity and Sensivity of rGO-FET Biosensor

The capacity of a reduced graphene oxide (rGO) field-effect transistor (FET) biosensor to selectively detect and distinguish a particular target analyte from other compounds present in a sample is referred to as specificity. It is crucial for biosensors to guarantee precise and trustworthy detection. To do so, the non-complementary sequence was dropped onto rGO that functionalized with probe sequence that match with miRNA-155 sequence. As seen in Figure 4.16, the Dirac point voltage was clearly showed very little shift which is 0.05 V. This neglectable shifts can explain with non-specific binding of miRNA-155 probe sequence and non-complementary probe sequences. Besides, the similar experienced results of this kind of deviation can be found in works of Cai et. al. (Cai et al., 2014, 2022). The capacity of a rGO-FET biosensor to selectively detect and distinguish a certain target analyte from other chemicals present in a sample is referred to as specificity. It is crucial for biosensors to guarantee precise and trustworthy detection.

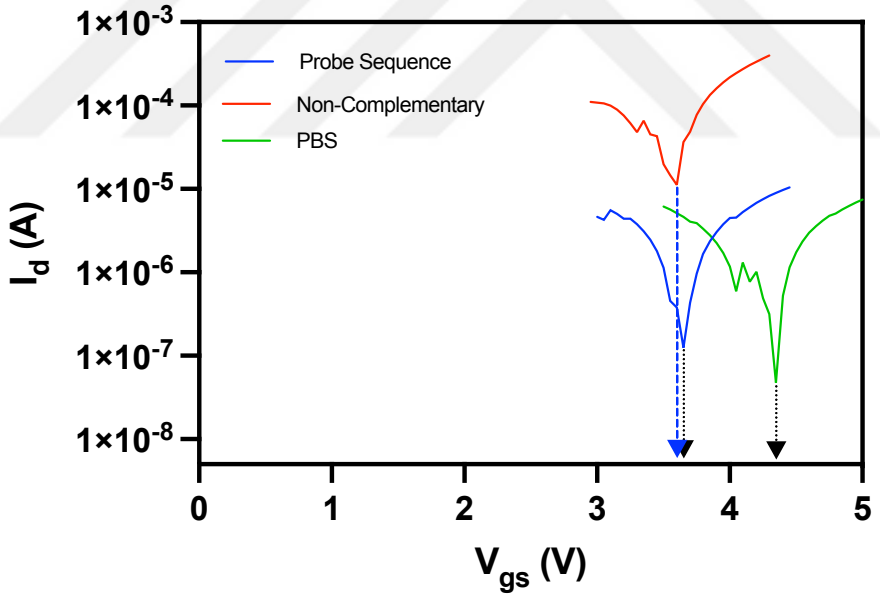

Figure 4.16. The I_d-V_{gs} curve of PBS, Probe Sequence and Non-Complementary Sequence.

The rGO-FET biosensor's sensitivity refers to its capacity to identify and measure minor variations in the target analyte's concentration or presence. It is a vital parameter that establishes the detection threshold and the biosensor's capacity to deliver readings that are accurate and trustworthy. In order to determine the sensivity of the fabricated rGO-FET device, the various concentration contained

miRNA-155 sequences was prepared. The concentration of prepared solution with miRNA-155 sequence as follows; 10 µM, 1 µM, 100 nM, and 100 pM. As seen in the Figure 4.17, while the concentration increases, the dirac point voltage shifts towards more lower voltages. The reason of the phenomenon is the negative particles in the solutions. The miRNA-155 with various concentration effectively interacted with graphene and impose the n-doping effect based on the reduced graphene oxide-nucleotide interaction (Cai et al., 2014, 2015, 2022; Gao et al., 2020). During measurement, it was also seen that the current values was changing. There are different possible reasons behind the change of current values as impurities caused by solutions, temperature and humidity, defects in rGO (Béraud et al., 2021; Bohunicky & Mousa, 2011; Novodchuk et al., 2021; Syu et al., 2018; Turner, 2013). The detectable lowest detection limit (LOD) was found as 100 pM in our study. In addition, it is significant to remember that a number of variables, including surface functionalization, temperature, pH, and the complexity of the sample matrix, can affect how sensitive rGO FET biosensors are. Because of this, extensive characterization and tuning are required to attain the optimum sensitivity for a given application.

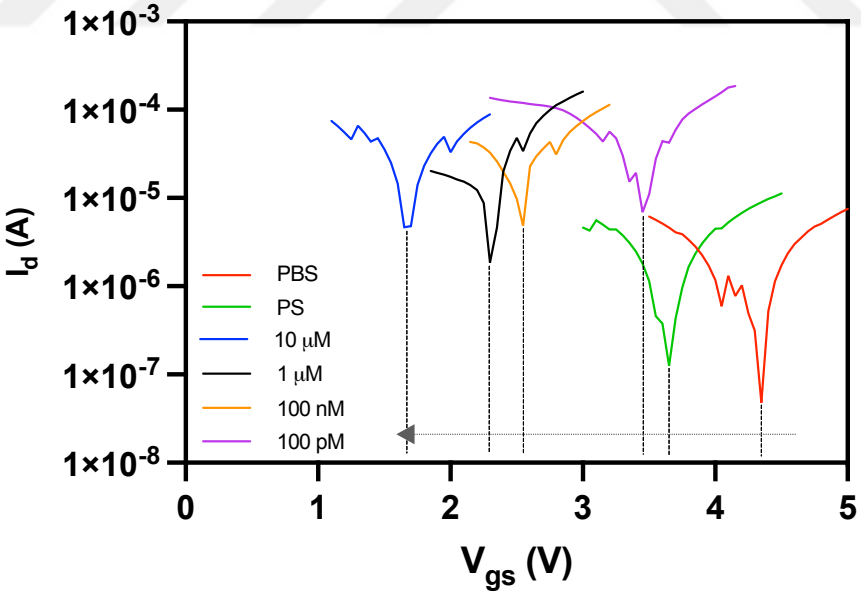

Figure 4.17. The I_d-V_{gs} transfer characteristics of rGO-FET biosensor with various concentration hybridization of miRNA-155 (PBS; Phosphate Buffered Saline, PS; Probe sequence, 10 µM; 10 µM miRNA-155 contained solution, 1 µM; 1 µM miRNA-155 contained solution, 100 nM; 100 nM miRNA-155 contained solution, 100 pM; 100 pM miRNA-155 contained solution).

In literature, there are many studies for the detection of miRNA-155 with various methods. The study of Hu et al. found that the lowest limit detection as 0.14 fM with carbon quantum dot (CQD) with functionalized with -NH_2 for immobilization of miRNA-155 (Hu et al., 2016), Wang et al. used paper-based biosensor for miRNA-155 detection with 0.67 pM LOD in their papers (F. Wang et al., 2020), Azimzadeh et. al. found that 0.6 fM LOD for miRNA-155 with graphene oxide and gold nanorod based biosensor (Azimzadeh et al., 2016) Hakimian et. al. found the lowest detection limit as 100 aM with positively charged Au nanoparticle based optical biosensor (Hakimian et al., 2018), Cardoso et al found that 5.7 aM limit of detection in their study with gold screen printed electrode biosensor (Cardoso et al., 2016), Liu et al in their work revealed that the lowest detection limit as 0.32 fM with FTO based biosensor (L. Liu et al., 2019), Majd et al used MoS_2 based FET biosensor and found the 0.03 fM LOD in their work (Majd et al., 2018), Yazdanparast et al found out that the lowest detection limit was 0.15 fM with their magneticcore-shell nanoparticles (Yazdanparast et al., 2020). Comparing these results with ours, the literature studies showed much lower limit of detection. However, most studies used different kind of biosensors in their work. We believe that, this study is the first conducted study for miRNA-155 detection for lymphoma cancer with reduced graphene oxide field effect transistor. We know that from all characterization our device has some disadvantages. With optimization, we believe that our proposed rGO-FET biosensor device detects lower concentration miRNA-155 for lymphoma cancer. Besides, all of our findings provide experimental evidence for the use of miR-155 as a potential blood-based biomarker related to cancer development and progression with rGO-FET biosensor.

4.3 Packaging and Reader Circuit of rGO-FET Biosensor

Even if it is not part of thesis, the packaging and instrumentation of rGO-FET biosensor devices were conducted. For the packaging, the PCBs were designed according to biosensor's contact probes which are source, drain and gate. As seen in Picture 4.2, after completion of contact we covered epoxy on top of wires to prevent breaking. The ugly prototype of reader circuit of rGO-FET device was designed and produced by Dr. Nikola Vasovic (Picture 4.3) who is currently working at Tyndall National Institute, Ireland. After completion of ugly prototype, only pH trials were terminated. In future, this prototype can be used as POC device in any environment after optimization and clinical tests of rGO-FET devices.

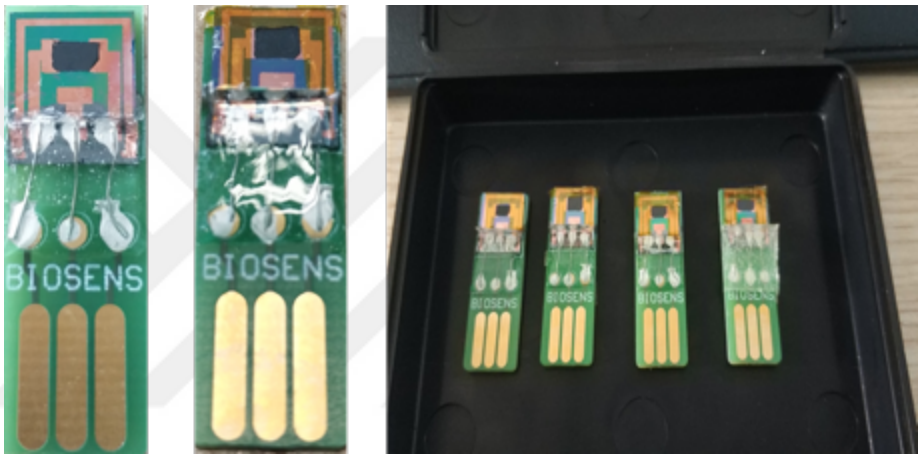

Picture 4.2 The packaged rGO-FET biosensor devices.

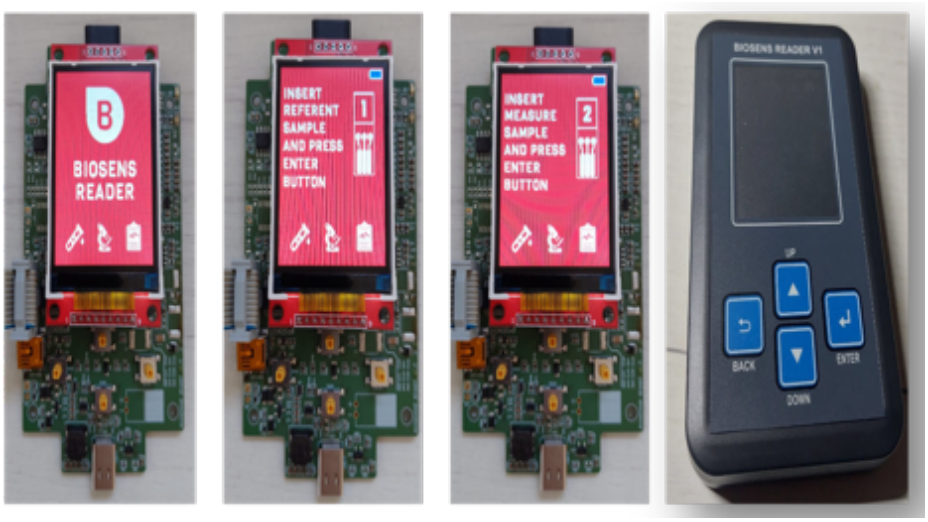

Picture 4.3. The reader circuit for rGO-FET Devices.

5. CONCLUSIONS AND RECOMMENDATIONS

In the conducted study, the rGO-FET biosensors were successfully fabricated and for the application both pH and miRNA-155 for early lymphoma cancer detection studies has been completed. The characteristics of the rGO revealed that exfoliation of reduced graphene oxide was done by firstly oxidation with Hummer's method and then chemical reduction with LAA. The characterization techniques showed the synthesized rGO consists of few layers and can be used for FET-based biosensor as transducer material. During experimental parts, the ultrasonic assisted coating method showed applicability when fabricating graphene FET-based biosensor for diagnostic features. Right after fabrication, the electrical characteristic of rGO-FET biosensor device has been completed via pH sensing capabilities and miRNA detections. Firstly, pH trials revealed that the fabricated rGO-FET biosensor has p-doped characteristics and with the changing pH values, the Dirac point voltage also changes. The result of such change showed us the applicability of rGO-FET biosensor for further investigations. For the miRNA detections, the immobilization of probe sequences has been completed on rGO layer. The electrical results showed that the difference in Dirac point voltage between blank measurement (with PBS) and probe sequence after immobilization. To detect miRNA-155, the hybridization was provided by dropping miRNA-155 sequence onto probe sequence with various concentrations. The I-V curves of rGO-FET biosensor devices displayed different voltage values during measurements. Lowest detection limit was determined as 100 pM with fabricated rGO-FET biosensor and the sensivity of the device showed that there was no any shift when experimenting with non-complementary sequence. Also, we believe that the comparison of the literature works of miRNA detection revealed this is the first study which uses miRNA and FET-based biosensor for early detection of lymphoma cancer and cancer metastasis. However, the results also showed that further optimization and examination have to be done for before clinical test. In below future recommendations can be found.

The future study recommendations for rGO-FET biosensor device:

1. **The optimization of mask design;**

The mask that used in conducted study was made printed onto acetate paper and applied with mask aligner system. Therefore, usage of acetate paper creates defects especially on the corners of the electrodes. This causes noise during electrical measurements. The proper chrome mask may reduce the defects on the corner of electrodes. This may reduce the signal-noise ratio.

2. **The optimization of reduced graphene oxide channel dimensions;**

The coated area with rGO in the conducted study is much larger comparing to literature works. This large area coating is also related with mask design. With the proper mask design, the coating area can be reduced into smaller size. With the scaling of rGO layer dimensions, the dimension of whole rGO-FET biosensor will be scaled down. The scaling of rGO-FET biosensor device will improve the integrability of the device with circuit reader systems. Also, in the conducted study, the coating method of rGO is new approach considering literature works. However, if possible, with the proper equipment such as oxygen plasma system, the scaling of rGO layer will be more controllable.

3. **Doping of rGO with metals;**

The rGO material can be modified for functionalization of biomarkers. During experiments, the functionalization of probe sequence, miRNA-155 sequence and non-complementary sequence was done directly. However, to increase the absorption of molecules onto rGO, some metals like gold, silver can be doped into rGO material. This may increase the functionalization of biomarkers and also increase the sensor performance by means of electrically.

4. **The linker material usage during immobilization of biomarkers;**

In literature, there are different linker molecules used for immobilization of various biomarkers such as PBASE. With the usage of linker materials, the sensivity, selectivity, stability and performance of rGO-FET biosensor may change.

5. **The usage of Ag/AgCl reference electrode;**

In our study, we conducted experiments with using Au/Ti electrodes for modulation of gate voltage. In literature, as reference electrode mostly Ag/AgCl electrode is preferred.

6. **Changing PBS solution concentration;**

The PBS solution that used during experiments has prepared as 10 mM. However, some studies showed that the changing molarity changes to ion concentration of the solution. Therefore, the effect of ion concentration in PBS also effects the performance of rGO-FET device. Hence, various concentrations of PBS solution can be examined in detail while determining of rGO-FET biosensor device.

7. **The PDMS microfluidic channel integration onto rGO layer;**

In the conducted study, the solution only dropped onto rGO layer by using micro pipette. The solution distributed unevenly on rGO and also some parts of solution gone onto Au/Ti metal contacts. This spread of solution causes noise while measuring. To prevent such issues, the microfluidic channel can be used instead of dropping solution directly onto rGO layer. The usage of microfluidic channel provides controllability of solution dropping. Also, the microfluidic channel provides more controllable sensing mechanism.

8. **The usage of other miRNAs related with Lymphoma Cancer;**

The sequence that used in the conducted study is miRNA-155 to detect lymphoma in early stages. However, the miRNA-155 is also considered for other cancer types such as breast cancer. To detect in early stages of lymphoma cancer the structure of rGO-FET biosensor can be optimized and with other related miRNA with Lymphoma cancer can be integrated onto same biosensor device. As a result, the rGO-FET biosensor's efficiency may be raised for the best available detection.

9. **The clinical tests with ethical permission;**

After completion of above-mentioned study to best optimized rGO-FET biosensor device, the clinical test has to be done for POC device for usage in hospitals or specialized laboratories. To do so, the ethical permission has to be taken from the council and required test should be terminated. Then, the POC device that fabricated can be useful tool for early diagnosis of lymphoma cancer and cancer metastasis.

6. REFERENCES

"APA citation system was used in this thesis."

Aamri, M. El, Yammouri, G., Mohammadi, H., Amine, A., & Korri-Youssoufi, H. (n.d.). *Electrochemical Biosensors for Detection of MicroRNA as a Cancer Biomarker: Pros and Cons*. https://doi.org/10.3390/bios10110186

Abdolhosseinzadeh, S., Asgharzadeh, H., & Kim, H. S. (2015). Fast and fully-scalable synthesis of reduced graphene oxide. *Scientific Reports*, *5*, 1–7. https://doi.org/10.1038/srep10160

Al-Mufti, S. M. S., Almontasser, A., & Rizvi, S. J. A. (2022). Influence of temperature variations on the dielectric parameters of thermally reduced graphene oxide. *Materials Today: Proceedings*, *57*, 1713–1718. https://doi.org/10.1016/j.matpr.2021.12.344

Andrijanto, E., Shoelarta, S., Subiyanto, G., & Rifki, S. (2016). Facile synthesis of graphene from graphite using ascorbic acid as reducing agent. *AIP Conference Proceedings*, *1725*(July). https://doi.org/10.1063/1.4945457

Andronescu, C., & Schuhmann, W. (2017). Graphene-based field effect transistors as biosensors. *Current Opinion in Electrochemistry*, *3*(1), 11–17. https://doi.org/10.1016/j.coelec.2017.03.002

Asakura, K., Kadota, T., Matsuzaki, J., Yoshida, Y., Yamamoto, Y., Nakagawa, K., Takizawa, S., Aoki, Y., Nakamura, E., Miura, J., Sakamoto, H., Kato, K., Watanabe, S., & Ochiya, T. (2020). A miRNA-based diagnostic model predicts resectable lung cancer in humans with high accuracy. *Communications Biology*, *3*(1), 134. https://doi.org/10.1038/s42003-020-0863-y

Asav, E., Sağiroğlu, A., & Sezgintürk, M. K. (2016). Quantitative Analysis of a Promising Cancer Biomarker, Calretinin, by a Biosensing System Based on Simple and Effective Immobilization Process. *Electroanalysis*, *28*(2), 334–342. https://doi.org/10.1002/elan.201500324

Aspermair, P., Mishyn, V., Bintinger, J., Happy, H., Bagga, K., Subramanian, P., Knoll, W., Boukherroub, R., & Szunerits, S. (2021). Reduced graphene oxide–based field effect transistors for the detection of E7 protein of human papillomavirus in saliva. *Analytical and Bioanalytical Chemistry*, *413*(3), 779–787. https://doi.org/10.1007/s00216-020-02879-z

Aspermair, P., Mishyn, V., Szunerits, S., & Knoll, W. (2020). Electronic biosensors based on graphene FETs. In *Methods in Enzymology* (1st ed., Vol. 642, pp. 371–401). Elsevier Inc. https://doi.org/10.1016/bs.mie.2020.05.016

Azimzadeh, M., Rahaie, M., Nasirizadeh, N., Ashtari, K., & Naderi-Manesh, H. (2016). An electrochemical nanobiosensor for plasma miRNA-155, based on graphene oxide and gold nanorod, for early detection of breast cancer. *Biosensors and Bioelectronics*, *77*, 99–106. https://doi.org/10.1016/J.BIOS.2015.09.020

Bai, Y., Xu, T., & Zhang, X. (2020). Graphene-based biosensors for detection of biomarkers. *Micromachines*, *11*(1). https://doi.org/10.3390/mi11010060

Balacescu, O., Visan, S., Baldasici, O., Balacescu, L., Vlad, C., & Achimas-Cadariu, P. (2019). MiRNA-Based Therapeutics in Oncology, Realities, and Challenges. *Antisense Therapy*. https://doi.org/10.5772/intechopen.81847

Balaji, A., & Zhang, J. (2017). Electrochemical and optical biosensors for early-stage cancer diagnosis by using graphene and graphene oxide. *Cancer Nanotechnology*, *8*(1). https://doi.org/10.1186/s12645-017-0035-z

Bedewy, A. M. L., Elmaghraby, S. M., Shehata, A. A., & Kandil, N. S. (2017). Prognostic value of miRNA-155 expression in B-cell Non-Hodgkin's lymphoma. *Turkish Journal of Hematology*, *34*(3), 207–212. https://doi.org/10.4274/tjh.2016.0286

Bellassai, N., & Spoto, G. (2016). Biosensors for liquid biopsy: circulating nucleic acids to diagnose and treat cancer. *Analytical and Bioanalytical Chemistry*, *408*(26), 7255–7264. https://doi.org/10.1007/s00216-016-9806-3

Bera, M., Chandravati, Gupta, P., & Maji, P. K. (2017). Facile One-Pot Synthesis of Graphene Oxide by Sonication Assisted Mechanochemical Approach and Its Surface Chemistry. *Journal of Nanoscience and Nanotechnology*, *18*(2), 902–912. https://doi.org/10.1166/jnn.2018.14306

Béraud, A., Sauvage, M., Bazán, C. M., Tie, M., Bencherif, A., & Bouilly, D. (2021). Graphene field-effect transistors as bioanalytical sensors: Design, operation and performance. *Analyst*, *146*(2), 403–428. https://doi.org/10.1039/d0an01661f

Bhalla, N., Jolly, P., Formisano, N., & Estrela, P. (2016a). Introduction to biosensors. *Essays in Biochemistry*, *60*(1), 1–8. https://doi.org/10.1042/EBC20150001

Bhalla, N., Jolly, P., Formisano, N., & Estrela, P. (2016b). Introduction to biosensors. *Essays in Biochemistry*, 60–61. https://doi.org/10.1042/EBC20150001

Bleu, Y., Bourquard, F., Loir, A., Barnier, V., Garrelie, F., & Donnet, C. (2019). Raman study of the substrate influence on graphene synthesis using a solid carbon source via rapid thermal annealing. *Journal of Raman Spectroscopy*, *50*(11), 1630–1641. https://doi.org/10.1002/jrs.5683

Bobrinetskiy, I. I., & Knezevic, N. Z. (2018). Graphene-based biosensors for on-site detection of contaminants in food. *Analytical Methods*, *10*(42), 5061–5070. https://doi.org/10.1039/c8ay01913d

Bohunicky, B., & Mousa, S. A. (2011). Biosensors: The new wave in cancer diagnosis. *Nanotechnology, Science and Applications*, *4*(1), 1–10. https://doi.org/10.2147/NSA.S13465

Bonavolontà, C., Vettoliere, A., Falco, G., Aramo, C., Rendina, I., Ruggiero, B., Silvestrini, P., & Valentino, M. (2021). Reduced graphene oxide on silicon-based structure as novel broadband photodetector. *Scientific Reports*, *11*(1), 1–10. https://doi.org/10.1038/s41598-021-92518-z

Boukhoubza, I., Khenfouch, M., Achehboune, M., Mothudi, B. M., Zorkani, I., & Jorio, A. (2019). X-ray diffraction investigations of nanostructured ZnO coated with reduced graphene oxide. *Journal of Physics: Conference Series*, *1292*(1). https://doi.org/10.1088/1742-6596/1292/1/012011

Cai, B., Huang, L., Zhang, H., Sun, Z., Zhang, Z., & Zhang, G. J. (2015). Gold nanoparticles-decorated graphene field-effect transistor biosensor for femtomolar MicroRNA detection. *Biosensors and Bioelectronics*, *74*, 329–334. https://doi.org/10.1016/J.BIOS.2015.06.068

Cai, B., Wang, S., Huang, L., Ning, Y., Zhang, Z., & Zhang, G. J. (2014). Ultrasensitive label-free detection of PNA-DNA hybridization by reduced graphene oxide field-effect transistor biosensor. *ACS Nano*, *8*(3), 2632–2638. https://doi.org/10.1021/nn4063424

Cai, B., Xia, Z., Wang, J., Wu, S., & Jin, X. (2022). Reduced Graphene Oxide-Based Field Effect Transistor Biosensors for High-Sensitivity miRNA21 Detection. *ACS Applied Nano Materials*, *5*(8), 12035–12044. https://doi.org/10.1021/acsanm.2c03372

Campos, R., Borme, J., Guerreiro, J. R., Machado, G., Cerqueira, M. F., Petrovykh, D. Y., & Alpuim, P. (2019). Attomolar label-free detection of dna hybridization with electrolyte-gated graphene field-effect transistors. *ACS Sensors*, *4*(2), 286–293. https://doi.org/10.1021/acssensors.8b00344

Cardoso, A. R., Moreira, F. T. C., Fernandes, R., & Sales, M. G. F. (2016). Novel and simple electrochemical biosensor monitoring attomolar levels of miRNA-155 in breast cancer. *Biosensors and Bioelectronics*, *80*, 621–630. https://doi.org/10.1016/J.BIOS.2016.02.035

Chandra, P., & Nee, Y. (n.d.). *Next Generation Point- of-care Biomedical Sensors Technologies for Cancer Diagnosis*.

Chen, X., Pu, H., Fu, Z., Sui, X., Chang, J., Chen, J., & Mao, S. (2018). Real-time and selective detection of nitrates in water using graphene-based field-effect transistor sensors. *Environmental Science: Nano*, *5*(8), 1990–1999. https://doi.org/10.1039/c8en00588e

Chen, Y. X., Huang, K. J., & Niu, K. X. (2018). Recent advances in signal amplification strategy based on oligonucleotide and nanomaterials for microRNA detection-a review. *Biosensors & Bioelectronics*, *99*, 612–624. https://doi.org/10.1016/J.BIOS.2017.08.036

Chiu, N.-F. (2022). The Current Status and Future Promise of SPR Biosensors. *Biosensors*, *12*(11), 933. https://doi.org/10.3390/bios12110933

Chuah, R., Gopinath, S. C. B., Anbu, P., Salimi, M. N., Yaakub, A. R. W., & Lakshmipriya, T. (2020). Synthesis and characterization of reduced graphene oxide using the aqueous extract of Eclipta prostrata. *3 Biotech*, *10*(8), 364. https://doi.org/10.1007/s13205-020-02365-4

Clark, L. C., & Lyons, C. (1962). Electrode Systems for Continuous Monitoring in Cardiovascular Surgery. *Annals of the New York Academy of Sciences*, *102*(1), 29–45. https://doi.org/10.1111/j.1749-6632.1962.tb13623.x

Coradduzza, D., Solinas, T., Balzano, F., Culeddu, N., Rossi, N., Cruciani, S., Azara, E., Maioli, M., Zinellu, A., De Miglio, M. R., Madonia, M., Falchi, M., & Carru, C. (2022). miRNAs as Molecular Biomarkers for Prostate Cancer. *Journal of Molecular Diagnostics*, *24*(11), 1171–1180. https://doi.org/10.1016/j.jmoldx.2022.05.005

De Micheli, G., Boero, C., Baj-Rossi, C., Taurino, I., & Carrara, S. (2012). Integrated biosensors for personalized medicine. *Proceedings of the 49th Annual Design Automation Conference on - DAC '12*, 6. https://doi.org/10.1145/2228360.2228363

Drees, E. E. E., & Pegtel, D. M. (2020). Circulating miRNAs as Biomarkers in Aggressive B Cell Lymphomas. In *Trends in Cancer* (Vol. 6, Issue 11, pp. 910–923). Cell Press. https://doi.org/10.1016/j.trecan.2020.06.003

Due, H., Svendsen, P., Bødker, J. S., Schmitz, A., Bøgsted, M., Johnsen, H. E., El-Galaly, T. C., Roug, A. S., & Dybkær, K. (2016). MiR-155 as a Biomarker in B-Cell Malignancies. *BioMed Research International*, *2016*. https://doi.org/10.1155/2016/9513037

Eis, P. S., Tam, W., Sun, L., Chadburn, A., Li, Z., Gomez, M. F., Lund, E., & Dahlberg, J. E. (2005). *Accumulation of miR-155 and BIC RNA in human B cell lymphomas*. https://www.pnas.org

Fales, A. (2014). Biosensors for Medical Applications. In *Biomedical Photonics Handbook, Second Edition* (pp. 3–46). CRC Press. https://doi.org/10.1201/b17289-3

Faniyi, I. O., Fasakin, O., Olofinjana, B., Adekunle, A. S., Oluwasusi, T. V., Eleruja, M. A., & Ajayi, E. O. B. (2019). The comparative analyses of reduced graphene oxide (RGO) prepared via green, mild and chemical approaches. *SN Applied Sciences*, *1*(10), 1–7. https://doi.org/10.1007/s42452-019-1188-7

Ferlay J, Ervik M, Lam F, Colombet M, Mery L, Piñeros M, Znaor A, Soerjomataram I, & Bray F. (2020). Global Cancer Observatory: Cancer Today. *International Agency for Research on Cancer*, *68*(6), 3–4. https://gco.iarc.fr/today

Fernandez-Mercado, M., Manterola, L., & Lawrie, C. (2015). MicroRNAs in Lymphoma: Regulatory Role and Biomarker Potential. *Current Genomics*, *16*(5), 349–358. https://doi.org/10.2174/1389202916666150707160147

Fu, W., Jiang, L., van Geest, E. P., Lima, L. M. C., & Schneider, G. F. (2017). Sensing at the Surface of Graphene Field-Effect Transistors. *Advanced Materials*, *29*(6). https://doi.org/10.1002/adma.201603610

Gao, J., Gao, Y., Han, Y., Pang, J., Wang, C., Wang, Y., Liu, H., Zhang, Y., & Han, L. (2020). Ultrasensitive Label-free MiRNA Sensing Based on a Flexible Graphene Field-Effect Transistor without Functionalization. *ACS Applied Electronic Materials*, *2*(4), 1090–1098. https://doi.org/10.1021/acsaelm.0c00095

GLOBOCAN. (2020). Non-Hodgkin lymphoma fact sheet. *Iarc*, *49*(5), 293–300.

Gürer, U., Yilmaz, O., Budak, E., & Yilmaz, E. (2022). THE COATING OF REDUCED GRAPHENE OXIDE (rGO): A NOVEL ULTRASONIC-ASSISTED METHOD. *RAP Conference Proceedings*. https://doi.org/10.37392/RapProc.2022.12

Habte, A. T., & Ayele, D. W. (2019). Synthesis and Characterization of Reduced Graphene Oxide (rGO) Started from Graphene Oxide (GO) Using the Tour Method with Different Parameters. *Advances in Materials Science and Engineering*, *2019*, 1–9. https://doi.org/10.1155/2019/5058163

Hakimian, F., Ghourchian, H., Hashemi, A. S., Arastoo, M. R., & Behnam Rad, M. (2018). Ultrasensitive optical biosensor for detection of miRNA-155 using positively charged Au nanoparticles. *Scientific Reports 2018 8:1*, *8*(1), 1–9. https://doi.org/10.1038/s41598-018-20229-z

Hamed, H., Elgammal, S., Narouz, M., & Elnaggar, M. (2021). Micro-RNA 155 in non-Hodgkin lymphoma. *The Egyptian Journal of Haematology*, *46*(1), 48. https://doi.org/10.4103/ejh.ejh_4_20

Hao, Z., Pan, Y., Huang, C., Wang, Z., Lin, Q., Zhao, X., & Liu, S. (2020). Modulating the Linker Immobilization Density on Aptameric Graphene Field Effect Transistors Using an Electric Field. *ACS Sensors*, *5*(8), 2503–2513. https://doi.org/10.1021/acssensors.0c00752

Hasegawa, M., Hirayama, Y., Ohno, Y., Maehashi, K., & Matsumoto, K. (2014). Characterization of reduced graphene oxide field-effect transistor and its application to biosensor. *Japanese Journal of Applied Physics*, *53*(5S1), 05FD05. https://doi.org/10.7567/JJAP.53.05FD05

Hidayah, N. M. S., Liu, W. W., Lai, C. W., Noriman, N. Z., Khe, C. S., Hashim, U., & Lee, H. C. (2017). Comparison on graphite, graphene oxide and reduced graphene oxide: Synthesis and characterization. *AIP Conference Proceedings*, *1892*. https://doi.org/10.1063/1.5005764

Hideshima, S., Hayashi, H., Takeuchi, R., Wustoni, S., Kuroiwa, S., Nakanishi, T., Momma, T., & Osaka, T. (2022). Improvement in long-term stability of field effect transistor biosensor in aqueous environments using a combination of silane and reduced graphene oxide coating. *Microelectronic Engineering*, *264*. https://doi.org/10.1016/j.mee.2022.111859

Hu, T., Zhang, L., Wen, W., Zhang, X., & Wang, S. (2016). Enzyme catalytic amplification of miRNA-155 detection with graphene quantum dot-based electrochemical biosensor. *Biosensors and Bioelectronics*, *77*, 451–456. https://doi.org/10.1016/J.BIOS.2015.09.068

Ickecan, D., Zan, R., & Nezir, S. (2017). Eco-Friendly Synthesis and Characterization of Reduced Graphene Oxide. *Journal of Physics: Conference Series*, *902*(1). https://doi.org/10.1088/1742-6596/902/1/012027

Ivnitski, D., Abdel-Hamid, I., Atanasov, P., & Wilkins, E. (1999). Biosensors for detection of pathogenic bacteria. *Biosensors and Bioelectronics*, *14*(7), 599–624. https://doi.org/10.1016/S0956-5663(99)00039-1

Ivnitski, D., Abdel-Hamid, I., Atanasov, P., Wilkins, E., & Stricker, S. (2000). Application of electrochemical biosensors for detection of food pathogenic bacteria. In *Electroanalysis*. https://doi.org/10.1002/(SICI)1521-4109(20000301)12:5<317::AID-ELAN317>3.0.CO;2-A

Jeong, J. T., Choi, M. K., Sim, Y., Lim, J. T., Kim, G. S., Seong, M. J., Hyung, J. H., Kim, K. S., Umar, A., & Lee, S. K. (2016). Effect of graphene oxide ratio on the cell adhesion and growth behavior on a graphene oxide-coated silicon substrate. *Scientific Reports*, *6*(May), 1–10. https://doi.org/10.1038/srep33835

Jin, X., Zhang, H., Li, Y. T., Xiao, M. M., Zhang, Z. L., Pang, D. W., Wong, G., Zhang, Z. Y., & Zhang, G. J. (2019). A field effect transistor modified with reduced graphene oxide for immunodetection of Ebola virus. *Microchimica Acta*, *186*(4). https://doi.org/10.1007/s00604-019-3256-5

Johnson, B. N., & Mutharasan, R. (2014). Biosensor-based microRNA detection: Techniques, design, performance, and challenges. *Analyst*, *139*(7), 1576–1588. https://doi.org/10.1039/c3an01677c

Kaisti, M. (2017). Detection principles of biological and chemical FET sensors. In *Biosensors and Bioelectronics* (Vol. 98, pp. 437–448). Elsevier. https://doi.org/10.1016/j.bios.2017.07.010

Karunakaran, C., Rajkumar, R., & Bhargava, K. (2015). Introduction to Biosensors. In *Biosensors and Bioelectronics*. Elsevier Inc. https://doi.org/10.1016/B978-0-12-803100-1.00001-3

Kim, H. E., Schuck, A., Lee, J. H., & Kim, Y. S. (2019). Solution-gated graphene field effect transistor for TP53 DNA sensor with coplanar electrode array. *Sensors and Actuators, B: Chemical*, *291*(March), 96–101. https://doi.org/10.1016/j.snb.2019.03.080

Kim, J. Y., Choi, K., Moon, D. Il, Ahn, J. H., Park, T. J., Lee, S. Y., & Choi, Y. K. (2013). Surface engineering for enhancement of sensitivity in an underlap-FET biosensor by control of wettability. *Biosensors and Bioelectronics*, *41*(1), 867–870. https://doi.org/10.1016/j.bios.2012.08.036

Kireev, D., Brambach, M., Seyock, S., Maybeck, V., Fu, W., Wolfrum, B., & Offenhaüsser, A. (2017). Graphene transistors for interfacing with cells: Towards a deeper understanding of liquid gating and sensitivity. *Scientific Reports*, *7*(1), 1–12. https://doi.org/10.1038/s41598-017-06906-5

Kong, W. Y., Wu, G. A., Wang, K. Y., Zhang, T. F., Zou, Y. F., Wang, D. D., & Luo, L. B. (2016). Graphene-β-Ga2O3Heterojunction for Highly Sensitive Deep UV Photodetector Application. *Advanced Materials*, *28*(48), 10725–10731. https://doi.org/10.1002/adma.201604049

Kumar, V., Kumar, A., Lee, D. J., & Park, S. S. (2021). Estimation of number of graphene layers using different methods: A focused review. In *Materials* (Vol. 14, Issue 16). MDPI AG. https://doi.org/10.3390/ma14164590

Kwong Hong Tsang, D., Lieberthal, T. J., Watts, C., Dunlop, I. E., Ramadan, S., del Rio Hernandez, A. E., & Klein, N. (2019a). Chemically Functionalised Graphene FET Biosensor for the Label-free Sensing of Exosomes. *Scientific Reports*, *9*(1). https://doi.org/10.1038/s41598-019-50412-9

Kwong Hong Tsang, D., Lieberthal, T. J., Watts, C., Dunlop, I. E., Ramadan, S., del Rio Hernandez, A. E., & Klein, N. (2019b). Chemically Functionalised Graphene FET Biosensor for the Label-free Sensing of Exosomes. *Scientific Reports*, *9*(1), 13946. https://doi.org/10.1038/s41598-019-50412-9

Larrea, E., Sole, C., Manterola, L., Goicoechea, I., Armesto, M., Arestin, M., Caffarel, M., Araujo, A., Araiz, M., Fernandez-Mercado, M., & Lawrie, C. (2016). New Concepts in Cancer Biomarkers: Circulating miRNAs in Liquid Biopsies. *International Journal of Molecular Sciences*, *17*(5), 627. https://doi.org/10.3390/ijms17050627

Lawrie, C. H. (2013). MicroRNAs and lymphomagenesis: A functional review. *British Journal of Haematology*, *160*(5), 571–581. https://doi.org/10.1111/BJH.12157

Le, G. T. T., Chanlek, N., Manyam, J., Opaprakasit, P., Grisdanurak, N., & Sreearunothai, P. (2019). Insight into the ultrasonication of graphene oxide with strong changes in its properties and performance for adsorption applications. *Chemical Engineering Journal*, *373*(May), 1212–1222. https://doi.org/10.1016/j.cej.2019.05.108

Lerner, M. B., Pan, D., Gao, Y., Locascio, L. E., Lee, K. Y., Nokes, J., Afsahi, S., Lerner, J. D., Walker, A., Collins, P. G., Oegema, K., Barron, F., & Goldsmith, B. R. (2017). Large scale commercial fabrication of high quality graphene-based assays for biomolecule detection. *Sensors and Actuators, B: Chemical*, *239*, 1261–1267. https://doi.org/10.1016/j.snb.2016.09.137

Li, B., Pan, G., Avent, N. D., Lowry, R. B., Madgett, T. E., & Waines, P. L. (2015). Graphene electrode modified with electrochemically reduced graphene oxide for label-free DNA detection. *Biosensors and Bioelectronics*, *72*, 313–319. https://doi.org/10.1016/J.BIOS.2015.05.034

Li, J., Sun, Y., & You, L. (2011). *Fabrication and Characterization of Nano-FET Biosensors for Studying Osteocyte Mechanotransduction*.

Li, S., Huang, K., Fan, Q., Yang, S., Shen, T., Mei, T., Wang, J., Wang, X., Chang, G., & Li, J. (2019). Highly sensitive solution-gated graphene transistors for label-free DNA detection. *Biosensors and Bioelectronics*, *136*(February), 91–96. https://doi.org/10.1016/j.bios.2019.04.034

Li, Y., Umer, R., Samad, Y. A., Zheng, L., & Liao, K. (2013). The effect of the ultrasonication pre-treatment of graphene oxide (GO) on the mechanical properties of GO/polyvinyl alcohol composites. *Carbon*, *55*, 321–327. https://doi.org/10.1016/J.CARBON.2012.12.071

Li, Y., Wu, Q., Zhao, Y., Bai, Y., Chen, P., Xia, T., & Wang, D. (2014). Response of MicroRNAs to in vitro treatment with graphene oxide. *ACS Nano*, *8*(3), 2100–2110. https://doi.org/10.1021/nn4065378

Lim, H. J., Saha, T., Tey, B. T., Tan, W. S., & Ooi, C. W. (2020). Quartz crystal microbalance-based biosensors as rapid diagnostic devices for infectious diseases. *Biosensors and Bioelectronics*, *168*, 112513. https://doi.org/10.1016/j.bios.2020.112513

Liu, H. (2014). Modified Thermal Reduction of Graphene Oxide. *Engineering and Technology*, *January*, 1–221. http://www.intechopen.com/source/pdfs/15270/intech-thermal_reduction_of_graphene_oxide.pdf

Liu, L., Zhu, S., Wei, Y., Liu, X. L., Jiao, S., & Yang, J. (2019). Ultrasensitive detection of miRNA-155 based on controlled fabrication of AuNPs@MoS2 nanostructures by atomic layer deposition. *Biosensors and Bioelectronics*, *144*, 111660. https://doi.org/10.1016/J.BIOS.2019.111660

Lowe, B. M., Sun, K., Zeimpekis, I., Skylaris, C. K., & Green, N. G. (2017). Field-effect sensors-from pH sensing to biosensing: Sensitivity enhancement using streptavidin-biotin as a model system. *Analyst*, *142*(22), 4173–4200. https://doi.org/10.1039/c7an00455a

Majd, S. M., Salimi, A., & Ghasemi, F. (2018). An ultrasensitive detection of miRNA-155 in breast cancer via direct hybridization assay using two-dimensional molybdenum disulfide field-effect transistor biosensor. *Biosensors and Bioelectronics*, *105*, 6–13. https://doi.org/10.1016/J.BIOS.2018.01.009

Mehrotra, P. (2016). Biosensors and their applications – A review. *Journal of Oral Biology and Craniofacial Research*, *6*(2), 153–159. https://doi.org/10.1016/j.jobcr.2015.12.002

Mohammadnejad, J., Basirhaghighi, N., Yazdian, F., Pourmadadi, M., Shabani Shayeh C, J., Omidi, M., Mirshafiei, M., Rahdar, A., & Díez-Pascual, A. M. (2023). Electrochemical nanobiosensor based on reduced graphene oxide and gold nanoparticles for ultrasensitive detection of microRNA-128. *International Immunopharmacology*, *117*, 109960. https://doi.org/10.1016/j.intimp.2023.109960

Mohammadnejad, J., Basirhaghighi, N., Yazdian, F., Pourmadadi, M., shayeh, J. S., Omidi, M., Mirshafiei, M., Rahdar, A., & Díez-Pascual, A. M. (2023). Electrochemical nanobiosensor based on reduced graphene oxide and gold nanoparticles for ultrasensitive detection of microRNA-128. *International Immunopharmacology*, *117*(February), 109960. https://doi.org/10.1016/j.intimp.2023.109960

Mohanty, P., Chen, Y., Wang, X., Hong, M. K., Rosenberg, C. L., & Weaver, D. T. (2012). *Field Effect Transistor Nanosensor for Breast Cancer Diagnostics*. 1–19.

Muzyka, R., Drewniak, S., Pustelny, T., Chrubasik, M., & Gryglewicz, G. (2018). Characterization of graphite oxide and reduced graphene oxide obtained from different graphite precursors and oxidized by different methods using Raman spectroscopy. *Materials*, *11*(7). https://doi.org/10.3390/ma11071050

Myung, S., Solanki, A., Kim, C., Park, J., Kim, K. S., & Lee, K. B. (2011). Graphene-encapsulated nanoparticle-based biosensor for the selective detection of cancer biomarkers. *Advanced Materials*, *23*(19), 2221–2225. https://doi.org/10.1002/adma.201100014

Negahdary, M., & Angnes, L. (n.d.). *Application of electrochemical biosensors for the detection of microRNAs (miRNAs) related to cancer*. https://doi.org/10.1016/j.ccr.2022.214565

Novodchuk, I., Bajcsy, M., & Yavuz, M. (2021). Graphene-based field effect transistor biosensors for breast cancer detection: A review on biosensing strategies. *Carbon*, *172*, 431–453. https://doi.org/10.1016/j.carbon.2020.10.048

Novoselov, K. S., Geim, A. K., Morozov, S. V., Jiang, D., Zhang, Y., Dubonos, S. V., Grigorieva, I. V., & Firsov, A. A. (2004). Electric field in atomically thin carbon films. *Science*, *306*(5696), 666–669. https://doi.org/10.1126/science.1102896

Owji, E., Ostovari, F., & Keshavarz, A. (2022). Electro-thermal properties and characterization of the flexible polyurethane-graphene nanocomposite films. *Phys. Scr*, *97*, 105704. https://doi.org/10.1088/1402-4896/ac8c05

Palas, W., Saisriyoot, M., Prapainainar, P., & Dittanet, P. (2019). Electrochemical performance of reduced graphene oxide-silica composite in polyaniline. *Materials Today: Proceedings*, *17*, 1277–1283. https://doi.org/10.1016/j.matpr.2019.06.016

Park, D., Kim, J. H., Kim, H. J., Lee, D., Lee, D. S., Yoon, D. S., & Hwang, K. S. (2020). Multiplexed femtomolar detection of Alzheimer's disease biomarkers in biofluids using a reduced graphene oxide field-effect transistor. *Biosensors and Bioelectronics*, *167*, 112505. https://doi.org/10.1016/J.BIOS.2020.112505

Paulmurugan, R., Ajayan, P. M., & Liepmann, D. (n.d.). *Intracellular microRNA quantification in intact cells: a novel strategy based on reduced graphene oxide-based fluorescence quenching*. https://doi.org/10.1557/mrc.2018.120

Peña-Bahamonde, J., Nguyen, H. N., Fanourakis, S. K., & Rodrigues, D. F. (2018). Recent advances in graphene-based biosensor technology with applications in life sciences. *Journal of Nanobiotechnology*, *16*(1), 1–17. https://doi.org/10.1186/s12951-018-0400-z

Pérez-Martínez, P., Galvan-Miyoshi, J. M., & Ortiz-López, J. (2016). Ultrasonic cavitation effects on the structure of graphene oxide in aqueous suspension. *Journal of Materials Science*, *51*(24), 10782–10792. https://doi.org/10.1007/s10853-016-0290-0

Purwidyantri, A., Domingues, T., Borme, J., Guerreiro, J. R., Ipatov, A., Abreu, C. M., Martins, M., Alpuim, P., & Prado, M. (2021). *Influence of the Electrolyte Salt Concentration on DNA Detection with Graphene Transistors*. https://doi.org/10.3390/bios11010024

Rodrigues, T., Mishyn, V., Leroux, Y. R., Butruille, L., Woitrain, E., Barras, A., Aspermair, P., Happy, H., Kleber, C., Boukherroub, R., Montaigne, D., Knoll, W., & Szunerits, S. (2022). Highly performing graphene-based field effect transistor for the differentiation between mild-moderate-severe myocardial injury. *Nano Today*, *43*. https://doi.org/10.1016/j.nantod.2022.101391

Rosenfeld, A. B., Kaplan, G. I., Carolan, M. G., Allen, B. J., Maughan, R., Yudelev, M., Kota, C., & Coderre, J. (1996). Simultaneous macro and micro dosimetry with MOSFETs. *IEEE Transactions on Nuclear Science*, *43*(6), 2693–2700. https://doi.org/10.1109/23.556855

Saliminejad, K., Khorram Khorshid, H. R., Soleymani Fard, S., & Ghaffari, S. H. (2019). An overview of microRNAs: Biology, functions, therapeutics, and analysis methods. *Journal of Cellular Physiology*, *234*(5), 5451–5465. https://doi.org/10.1002/jcp.27486

Santangelo MF, C. S. (2014). Optical and Electrical Si-Based Biosensors: Fabrication and Trasduction Issues. *Journal of Analytical & Bioanalytical Techniques*, *s12*`(01). https://doi.org/10.4172/2155-9872.s12-007

Sarkar, D., Liu, W., Xie, X., Anselmo, A. C., Mitragotri, S., & Banerjee, K. (2014). MoS2 field-effect transistor for next-generation label-free biosensors. *ACS Nano*, *8*(4), 3992–4003. https://doi.org/10.1021/nn5009148

Sawant, S. N. (2017). Development of Biosensors From Biopolymer Composites. *Biopolymer Composites in Electronics*, 353–383. https://doi.org/10.1016/B978-0-12-809261-3.00013-9

Science, C., & Lu, X. (2018). *Reduced Graphene Oxide Biosensors for Prostate Cancer Biomarker Detection*.

Shabaninejad, Z., Yousefi, F., Movahedpour, A., Ghasemi, Y., Dokanehiifard, S., Rezaei, S., Aryan, R., Savardashtaki, A., & Mirzaei, H. (2019). Electrochemical-based biosensors for microRNA detection: Nanotechnology comes into view. In *Analytical Biochemistry* (Vol. 581). Academic Press Inc. https://doi.org/10.1016/j.ab.2019.113349

Sharifianjazi, F., Jafari Rad, A., Bakhtiari, A., Niazvand, F., Esmaeilkhanian, A., Bazli, L., Abniki, M., Irani, M., & Moghanian, A. (2022). Biosensors and nanotechnology for cancer diagnosis (lung and bronchus, breast, prostate, and colon): A systematic review. *Biomedical Materials (Bristol)*, *17*(1). https://doi.org/10.1088/1748-605X/ac41fd

Sharma, R., Chadha, N., & Saini, P. (2017). Determination of defect density, crystallite size and number of graphene layers in graphene analogues using X-ray diffraction and Raman spectroscopy. *Indian Journal of Pure & Applied Physics*, *55*, 625–629.

Shobha, B. N., & Muniraj, N. J. R. (2014). *Design, Modeling and Simulation of Prostate Cancer Biosensor with ssDNA biomarker and DGFET Biosensor*. *5*(2), 2612–2620. http://www.ijcsit.com/docs/Volume 5/vol5issue02/ijcsit20140502370.pdf

Shoorideh, K., & Chui, C. O. (2012). Optimization of the Sensitivity of FET-Based Biosensors via Biasing and Surface Charge Engineering. *IEEE Transactions on Electron Devices*, *59*(11), 3104–3110. https://doi.org/10.1109/TED.2012.2214221

Sieradzka, M., Ślusarczyk, C., Fryczkowski, R., & Janicki, J. (2020). Insight into the effect of graphite grain sizes on the morphology, structure and electrical properties of reduced graphene oxide. *Journal of Materials Research and Technology*, *9*(4), 7059–7067. https://doi.org/10.1016/j.jmrt.2020.05.026

Singh, A., Sharma, N., Arif, M., & Katiyar, R. S. (2019). Electrically reduced graphene oxide for photovoltaic application. *Journal of Materials Research*, *34*(4), 652–660. https://doi.org/10.1557/jmr.2019.32

Solé, C., Arnaiz, E., & Lawrie, C. H. (2018). MicroRNAs as Biomarkers of B-cell Lymphoma. *Biomarker Insights*, *13*. https://doi.org/10.1177/1177271918806840

Solé, C., Larrea, E., Di Pinto, G., Tellaexte, M., & Lawrie, C. H. (2017). miRNAs in B-cell lymphoma: Molecular mechanisms and biomarker potential. *Cancer Letters*, *405*, 79–89. https://doi.org/10.1016/j.canlet.2017.07.020

Sreejith, S., Ajayan, J., Radhika, J. M., Sivasankari, B., Tayal, S., & Saravanan, M. (2023). A comprehensive review on graphene FET bio-sensors and their emerging application in DNA/RNA sensing & rapid Covid-19 detection. *Measurement*, *206*, 112202. https://doi.org/10.1016/j.measurement.2022.112202

Syama, S., & Mohanan, P. V. (2019). Comprehensive Application of Graphene: Emphasis on Biomedical Concerns. *Nano-Micro Letters*, *11*(1), 6. https://doi.org/10.1007/s40820-019-0237-5

Syu, Y.-C., Hsu, W.-E., & Lin, C.-T. (2018). Review—Field-Effect Transistor Biosensing: Devices and Clinical Applications. *ECS Journal of Solid State Science and Technology*, *7*(7), Q3196–Q3207. https://doi.org/10.1149/2.0291807jss

Szunerits, S., & Boukherroub, R. (2018). Graphene-based biosensors. *Interface Focus*, *8*, 20160132.

Szunerits, S., Rodrigues, T., Bagale, R., Happy, H., Boukherroub, R., & Knoll, W. (2023). Graphene-based field-effect transistors for biosensing: where is the field heading to? *Analytical and Bioanalytical Chemistry*. https://doi.org/10.1007/s00216-023-04760-1

Taniselass, S., Md Arshad, M. K., & Gopinath, S. C. B. (2019). *Graphene-based electrochemical biosensors for monitoring noncommunicable disease biomarkers*. https://doi.org/10.1016/j.bios.2019.01.047

Tas, M., Altin, Y., & Celik Bedeloglu, A. (2019). Reduction of graphene oxide thin films using a stepwise thermal annealing assisted by L-ascorbic acid. *Diamond and Related Materials*, *92*(January), 242–247. https://doi.org/10.1016/j.diamond.2019.01.009

Thakur, A., Kumar, S., & Rangra, V. S. (2015). Synthesis of reduced graphene oxide (rGO) via chemical reduction. *AIP Conference Proceedings*, *1661*(Iccmp 2014), 1–6. https://doi.org/10.1063/1.4915423

Thévenot, D. R., Toth, K., Durst, R. A., Wilson, G. S., & Thévenot, D. R. (2001). Electrochemical biosensors: recommended definitions and classification. *Biosensors & Bioelectronics*, *16*, 121–131. www.elsevier.com/locate/bios

Tian, M., Qiao, M., Shen, C., Meng, F., Frank, L. A., Krasitskaya, V. V., Wang, T., Zhang, X., Song, R., Li, Y., Liu, J., Xu, S., & Wang, J. (2020). Highly-sensitive graphene field effect transistor biosensor using PNA and DNA probes for RNA detection. *Applied Surface Science*, *527*(June). https://doi.org/10.1016/j.apsusc.2020.146839

Tran, T. T., & Mulchandani, A. (2016). Carbon nanotubes and graphene nano field-effect transistor-based biosensors. *TrAC Trends in Analytical Chemistry*, *79*, 222–232. https://doi.org/10.1016/J.TRAC.2015.12.002

Tu, N. D. K., Choi, J., Park, C. R., & Kim, H. (2015). Remarkable Conversion Between n- and p-Type Reduced Graphene Oxide on Varying the Thermal Annealing Temperature. *Chemistry of Materials*, *27*(21), 7362–7369. https://doi.org/10.1021/acs.chemmater.5b02999

Turner, A. P. F. (2013). Biosensors: sense and sensibility. *Chemical Society Reviews*, *42*(8), 3184. https://doi.org/10.1039/c3cs35528d

Vasilijević, S., Boukraa, R., Battaglini, N., & Piro, B. (2023). Graphene-based materials and their applications in electrolyte-gated transistors for sensing. *Synthetic Metals*, *295*, 117355. https://doi.org/10.1016/j.synthmet.2023.117355

Velasco-Garcia, M. N., & Mottram, T. (2003). Biosensor technology addressing agricultural problems. *Biosystems Engineering*, *84*(1), 1–12. https://doi.org/10.1016/S1537-5110(02)00236-2

Verma, S., Das, T., Pandey, V. K., & Verma, B. (2022). Facile and scalable synthesis of reduced-graphene oxide using different green reducing agents and its characterizations. *Diamond and Related Materials*, *129*. https://doi.org/10.1016/J.DIAMOND.2022.109361

Viswanathan, S., Narayanan, T. N., Aran, K., Fink, K. D., Paredes, J., Ajayan, P. M., Filipek, S., Miszta, P., Tekin, H. C., Inci, F., Demirci, U., Li, P., Bolotin, K. I., Liepmann, D., &

Renugopalakrishanan, V. (2015). Graphene-protein field effect biosensors: Glucose sensing. In *Materials Today*. https://doi.org/10.1016/j.mattod.2015.04.003

von Lüders, L., Tilmann, R., Lee, K., Bartlam, C., Nevanen, T., Iljin, K., Knirsch, K. C., Hirsch, A., & Duesberg, G. S. (2023). Functionalisation of Graphene Sensor Surfaces for the Specific Detection of Biomarkers. *Angewandte Chemie International Edition*. https://doi.org/10.1002/anie.202219024

Wang, F., Fu, C., Huang, C., Li, N., Wang, Y., Ge, S., & Yu, J. (2020). Paper-based closed Au-Bipolar electrode electrochemiluminescence sensing platform for the detection of miRNA-155. *Biosensors and Bioelectronics*, *150*, 111917. https://doi.org/10.1016/J.BIOS.2019.111917

Wang, Y., Chen, Y., Lacey, S. D., Xu, L., Xie, H., Li, T., Danner, V. A., & Hu, L. (2018). Reduced graphene oxide film with record-high conductivity and mobility. *Materials Today*, *21*(2), 186–192. https://doi.org/10.1016/J.MATTOD.2017.10.008

Wang, Y., Xu, H., Zhang, J., & Li, G. (2008). Electrochemical sensors for clinic analysis. *Sensors*, *8*(4), 2043–2081. https://doi.org/10.3390/s8042043

Wen, P., Xie, Y., & Wang, L. (2021). The Role of microRNA in Pathogenesis, Diagnosis, Different Variants, Treatment and Prognosis of Mycosis Fungoides. *Frontiers in Oncology*, *11*. https://doi.org/10.3389/FONC.2021.752817/FULL

Wu, J. Bin, Lin, M. L., Cong, X., Liu, H. N., & Tan, P. H. (2018). Raman spectroscopy of graphene-based materials and its applications in related devices. *Chemical Society Reviews*, *47*(5), 1822–1873. https://doi.org/10.1039/c6cs00915h

Wu, X., Mu, F., Wang, Y., & Zhao, H. (2018). Graphene and graphene-based nanomaterials for DNA detection: A review. *Molecules*, *23*(8). https://doi.org/10.3390/molecules23082050

Xu, C., Shi, X., Ji, A., Shi, L., Zhou, C., & Cui, Y. (2015). Fabrication and characteristics of reduced graphene oxide produced with different green reductants. *PLoS ONE*, *10*(12). https://doi.org/10.1371/journal.pone.0144842

Yamada, K., Okamoto, M., Sakurai, M., Suenobu, T., & Nakayama, K. I. (2019). Solution-processable reduced graphene oxide template layer for molecular orientation control of organic semiconductors. *RSC Advances*, *9*(57), 32940–32945. https://doi.org/10.1039/c9ra06258k

Yan, H., Xu, Y., Lu, Y., & Xing, W. (2017). Reduced Graphene Oxide-Based Solid-Phase Extraction for the Enrichment and Detection of microRNA. *Analytical Chemistry*, *89*(19), 10137–10140. https://doi.org/10.1021/acs.analchem.7b03138

Yazdanparast, S., Benvidi, A., Azimzadeh, M., Tezerjani, M. D., & Ghaani, M. R. (2020). Experimental and theoretical study for miR-155 detection through resveratrol interaction with nucleic acids using magnetic core-shell nanoparticles. *Microchimica Acta*, *187*(8), 1–10. https://doi.org/10.1007/S00604-020-04447-9/TABLES/2

Yin, H. (2018). Application of graphene FET nucleic acid biosensor in human motion measurement. *International Journal Bioautomation*, *22*(Specialissue4), 337–348. https://doi.org/10.7546/ijba.2018.22.4.337-348

Yoo, H., Kim, Y., Lee, J., Lee, H., Yoon, Y., Kim, G., & Lee, H. (2012). N-type reduced graphene oxide field-effect transistors (Fets) from photoactive metal oxides. *Chemistry - A European Journal*, *18*(16), 4923–4929. https://doi.org/10.1002/chem.201103967

Yoon, J.-Y., & Kim, B. (2012). Lab-on-a-Chip Pathogen Sensors for Food Safety. *Sensors*, *12*(8), 10713–10741. https://doi.org/10.3390/s120810713

Zhang, X., Jing, Q., Ao, S., Schneider, G. F., Kireev, D., Zhang, Z., & Fu, W. (2020). Ultrasensitive Field-Effect Biosensors Enabled by the Unique Electronic Properties of Graphene. *Small*, *16*(15), 1–24. https://doi.org/10.1002/smll.201902820

ZHONG, H., XU, L., ZHONG, J.-H., XIAO, F., LIU, Q., HUANG, H.-H., & CHEN, F.-Y. (2012). Clinical and prognostic significance of miR-155 and miR-146a expression levels in formalin-fixed/paraffin-embedded tissue of patients with diffuse large B-cell lymphoma. *Experimental and Therapeutic Medicine*, *3*(5), 763–770. https://doi.org/10.3892/etm.2012.502

Zhou, Q., Qiu, Q., & Huang, Z. (2022). Graphene-based terahertz optoelectronics. *Optics & Laser Technology*, 108558. https://doi.org/10.1016/j.optlastec.2022.108558

Zuñiga, J., Akashi, L., Pinheiro, T., Rivera, M., Barreto, L., Albertin, K. F., & Champi, A. (2022). Synthesis of lysozyme-reduced graphene oxide films for biosensor applications. *Diamond and Related Materials*, *126*. https://doi.org/10.1016/j.diamond.2022.109093

7. APPENDICES

Appendix 1 The images of experimental works during synthesizing of reduced graphene oxide.

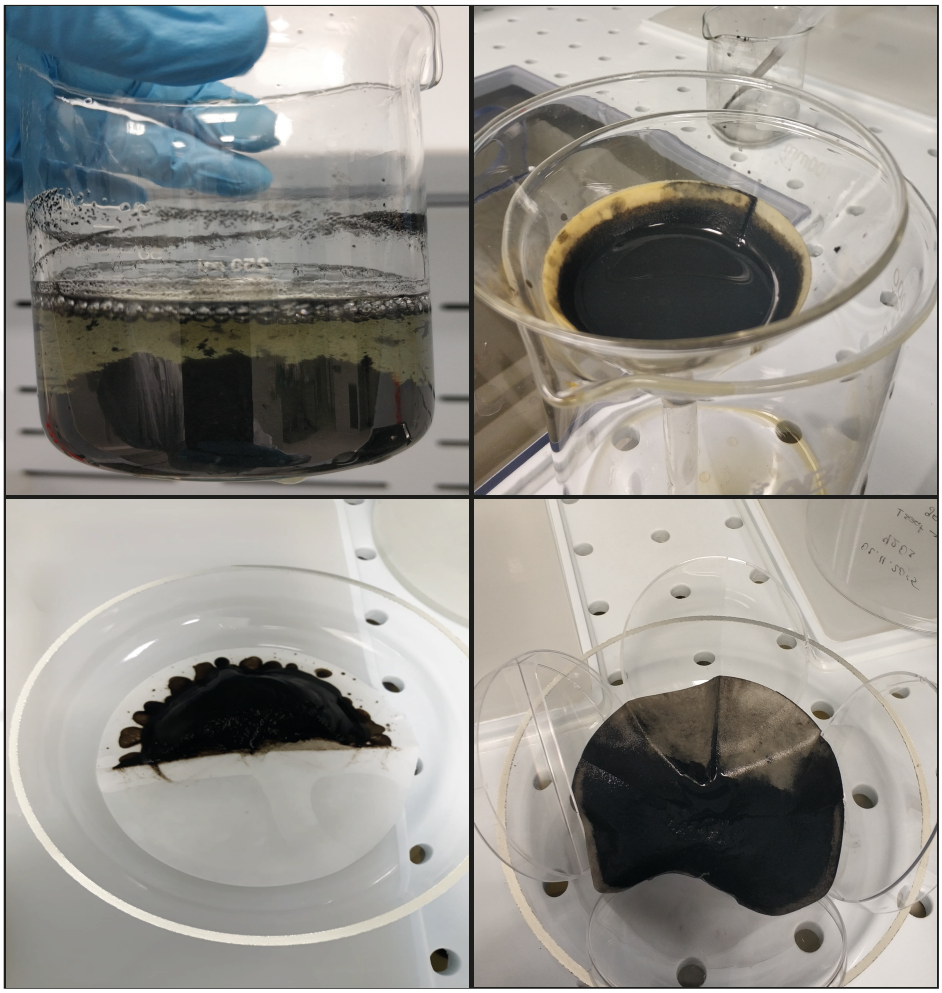

Appendix 2 The images of experimental works during fabrication of FET devices.